AD-A053 598 SYRACUSE UNIV N Y F/G 21/2
THE EFFECT OF A WIDE EXHAUST PLUME ON THE SCATTERING CURRENT OF--ETC(U)
MAR 78 H K SCHUMAN, V W EVELEIGH F30602-75-C-0121
UNCLASSIFIED RADC-TR-78-47 NL

| OF |
AD
A053598

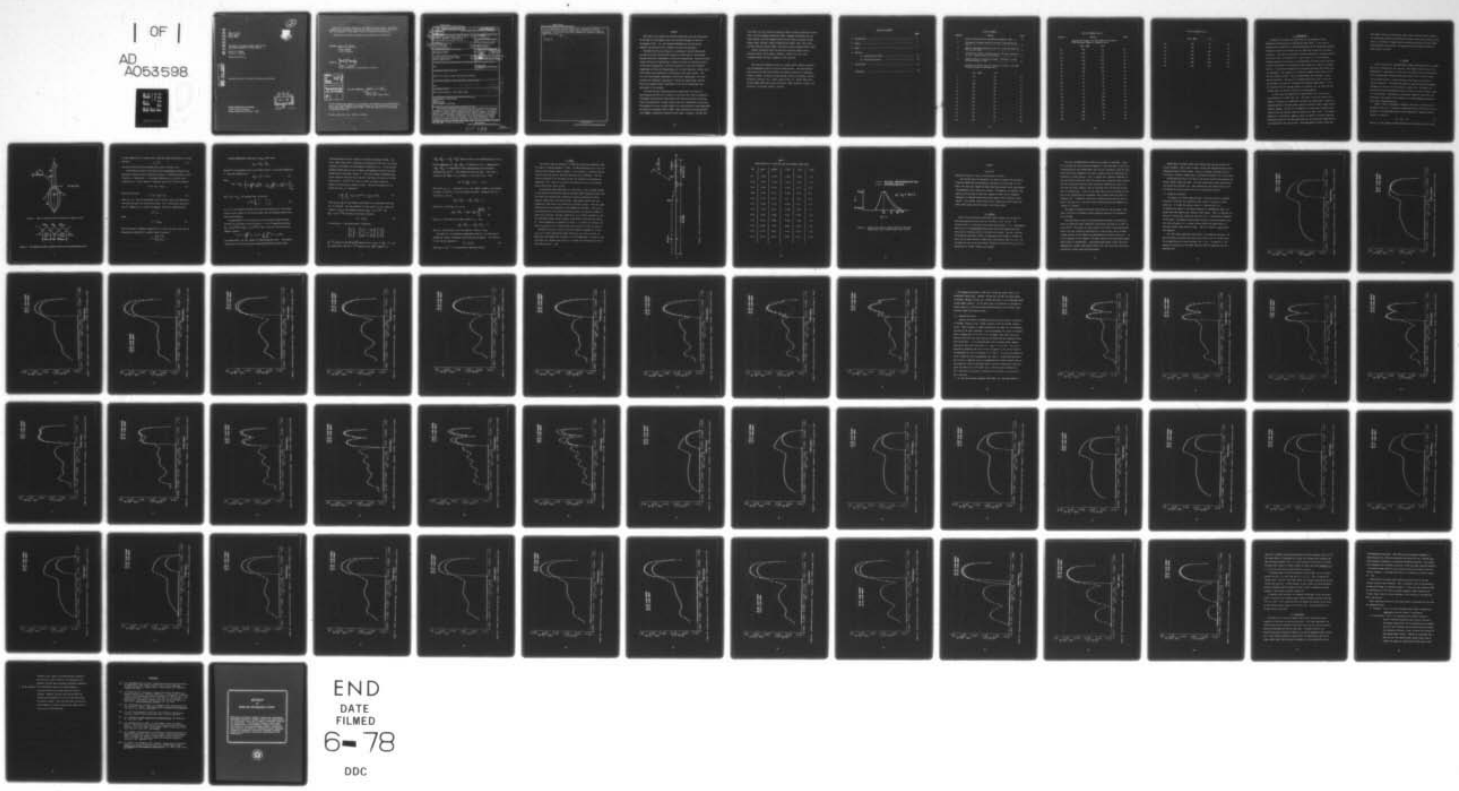

END
DATE
FILMED
6-78
DDC

RADC-TR-78-47
Phase Report
March 1978

THE EFFECT OF A WIDE EXHAUST PLUME ON THE SCATTERING CURRENT OF A THIN MISSILE

Harvey K. Schuman
Virgil W. Eveleigh

Syracuse University

ROME AIR DEVELOPMENT CENTER
Air Force Systems Command
Griffiss Air Force Base, New York 13441

This report has been reviewed by the RADC Information Office (OI) and is releasable to the National Technical Information Service (NTIS). At NTIS it will be releasable to the general public, including foreign nations.

RADC-TR-78-47 has been reviewed and is approved for publication.

APPROVED: Jacob Scherer

JACOB SCHERER
Project Engineer

APPROVED: Joseph J Naresky

JOSEPH J. NARESKY
Chief, Reliability & Compatibility Division

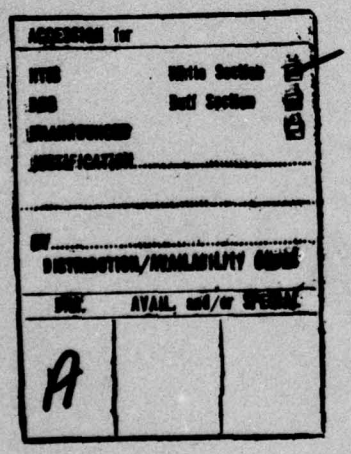

FOR THE COMMANDER: John P. Huss

JOHN P. HUSS
Acting Chief, Plans Office

If your address has changed or if you wish to be removed from the RADC mailing list, or if the addressee is no longer employed by your organization, please notify RADC (RBC) Griffiss AFB NY 13441. This will assist us in maintaining a current mailing list.

Do not return this copy. Retain or destroy.

UNCLASSIFIED

SECURITY CLASSIFICATION OF THIS PAGE (When Data Entered)

REPORT DOCUMENTATION PAGE

READ INSTRUCTIONS BEFORE COMPLETING FORM

1. REPORT NUMBER: RADC-TR-78-47	2. GOVT ACCESSION NO.
3. RECIPIENT'S CATALOG NUMBER	
4. TITLE (and Subtitle): THE EFFECT OF A WIDE EXHAUST PLUME ON THE SCATTERING CURRENT OF A THIN MISSILE.	5. TYPE OF REPORT & PERIOD COVERED: Phase Report.
6. PERFORMING ORG. REPORT NUMBER: N/A	
7. AUTHOR(s): Harvey K. Schuman, Virgil W. Eveleigh	8. CONTRACT OR GRANT NUMBER(s): F30602-75-C-0121
9. PERFORMING ORGANIZATION NAME AND ADDRESS: Syracuse University, Syracuse NY 13210	10. PROGRAM ELEMENT, PROJECT, TASK AREA & WORK UNIT NUMBERS: 95670016, 920W, 00
11. CONTROLLING OFFICE NAME AND ADDRESS: Rome Air Development Center (RBC), Griffiss AFB NY 13441	12. REPORT DATE: Mar 78; NUMBER OF PAGES: 60 (71 p.)
14. MONITORING AGENCY NAME & ADDRESS (if different from Controlling Office): Same	15. SECURITY CLASS. (of this report): UNCLASSIFIED
	15a. DECLASSIFICATION/DOWNGRADING SCHEDULE: N/A

16. DISTRIBUTION STATEMENT (of this Report)

Approved for public release; distribution unlimited.

17. DISTRIBUTION STATEMENT (of the abstract entered in Block 20, if different from Report)

Same

63203F

18. SUPPLEMENTARY NOTES

RADC Project Engineer: Jacob Scherer (RBC)

19. KEY WORDS (Continue on reverse side if necessary and identify by block number)

Electromagnetic Compatibility
Missile
Missile PLUME
Electromagnetic Scattering

20. ABSTRACT (Continue on reverse side if necessary and identify by block number)

Theoretical predictions of the plane-wave induced uniform-mode scattering current on a typical missile with exhaust plume are presented. An approximate mathematical model is derived based on body-of-revolution theory, the moment method, an impedance-sheet representation and recently achieved plume conductivity profiles. Particular attention is paid to the modification of missile current due to the presence of the plume. This effort supplements recently reported work based on thin-wire modeling of both missile and plume. The significant width of the plume, about eight times the missile diameter, warrents

DD FORM 1 JAN 73 1473 EDITION OF 1 NOV 65 IS OBSOLETE

UNCLASSIFIED

SECURITY CLASSIFICATION OF THIS PAGE (When Data Entered)

339 600

the more sophisticated modeling employed here. Frequencies considered correspond to missile electrical lengths approximately between 0.1 and 1.0 wavelengths. The excitation directions considered are between broadside and 15° off missile axis.

DEGREE

PREFACE

This effort was conducted by Syracuse University under the sponsorship of the Rome Air Development Center Post-Doctoral Program for Rome Air Development Center. Mr. Jack Edwards RADC/RBCA was the task project engineer and provided overall technical direction and guidance.

The RADC Post-Doctoral Program is a cooperative venture between RADC and some sixty-five universities eligible to participate in the program. Syracuse University (Department of Electrical Engineering), Purdue University (School of Electrical Engineering), Georgia Institute of Technology (School of Electrical Engineering), and State University of New York at Buffalo (Department of Electrical Engineering) act as prime contractor schools with other schools participating via sub-contracts with prime schools. The U.S. Air Force Academy (Department of Electrical Engineering), Air Force Institute of Technology (Department of Electrical Engineering), and the Naval Post Graduate School (Department of Electrical Engineering) also participate in the program.

The Post-Doctoral Program provides an opportunity for faculty at participating universities to spend up to one year full time on exploratory development and problem-solving efforts with the post-doctorals splitting their time between the customer location and their educational institutions. The program is totally customer-funded with current projects being undertaken for Rome Air Development Center (RADC), Space and Missile Systems Organization (SAMSO), Aeronautical System Division (ASD), Electronic Systems Divi-

sion (ESD), Air Force Avionics Laboratory (AFAL), Foreign Technology Division (FTD), Air Force Weapons Laboratory (AFWL), Armament Development and Test Center (ADTC), Air Force Communications Service (AFCS), Aerospace Defense Command (ADC), HQ USAF, Defense Communications Agency (DCA), Navy, Army, Aerospace Medical Division (AMD), and Federal Aviation Administration (FAA).

Further information about the RADC Post-Doctoral Program can be obtained from Mr. Jacob Scherer, RADC/RBC, Griffiss AFB, NY, 13441, telephone Autovon 587-2543, Commercial (315) 330-2543.

This work was performed as part of a larger effort aimed at analyzing the electromagnetic effect of missile exhaust plumes. The participating organizations for the overall effort are Georgia Institute of Technology, Atlanta, Georgia; University of Mississippi, Oxford, Mississippi; Syracuse University, Syracuse, N.Y.; RADC, Griffiss AFB, N.Y.: MICOM, Huntsville, Alabama; OMEW, WSMR, White Sands, New Mexico: NSWC, Dahlgren, Virginia; and University of Colorado, Boulder, Colorado.

TABLE OF CONTENTS

LIST OF FIGURES

LIST OF FIGURES (cont.)

LIST OF FIGURES (cont.)

1. INTRODUCTION

Currently of interest are predictions of electromagnetic field penetration within missiles irradiated by plane waves. A first step in obtaining such predictions is often determination of the scattering currents induced on the missile surfaces with all apertures covered over by perfect conductors. Then known relationships between apertureless scattering current and cavity field, as presented in a recent report [7], can be employed. Computed uniform (with respect to circumferential variation) mode scattering current distributions are presented in this report for a model of a typical missile. A variety of frequencies and incident plane-wave field directions are considered. Our purpose is to assess the exhaust plume effect on the missile surface currents. Thus a suitable model for the plume is given special attention. The missile is assumed electrically thin so only the uniform mode of current is considered in evaluating plume effects. It is not inferred that the induced currents are uniform, but only that the non-uniform modes are much less sensitive to plume presence.

A recent paper [8] addresses this plume effect for a missile-plus-plume modeled as a loaded thin wire. The plume is not truly needle thin, however, so analysis is needed which accounts for plume width. Results are reported herein as obtained using a body-of-revolution (BOR), moment method computer program. The missile is modeled as a conducting cylindrical tube closed at one end (missile nose) and open at the other (tail). The plume is modeled as a rotationally symmetric shell (or sheet) of resistive material. Theoretical bases for the BOR program and the resistive-sheet approximation are discussed in the next section. Then approximate resistive loads and

plume model contour are determined. These loads are derived from a theoretical conductivity profile of the missile's plume recently made available [6,8]. Finally, in Section 4 computed missile scattering currents with and without plume presence are presented. An evaluation of plume effects based upon these results is given.

2. Theory

A brief review of the Harrington-Mautz moment method modeling of a loaded BOR [1,2] is presented in this section. This method, based on an $\underset{\sim}{E}$-field formulation, is applicable to a wide class of radiation and scattering problems including those involving thin-walled bodies such as missile shells. Also included herein is a model derivation based upon a thin shell of resistive material. The derivation parallels that presented by Harrington and Mautz for the case of thin dielectric shells [3]. The method for determining approximate BOR model loads to account for this resistive sheet is also presented. Although only rotationally symmetric thin shells are considered, this theory can be extended to existing homogeneous material body surface formulations [4].

Figure 1 shows a rotationally symmetric thin shell of surface area S. The upper portion, S_c, is perfectly conducting and the lower portion, S_r, is resistive. The conducting portion may be replaced by a combined surface current, $\underset{\sim}{J}_c$, equal to

$$\underset{\sim}{J}_c = \underset{\sim}{J}_c^{+} + \underset{\sim}{J}_c^{-} \tag{1}$$

where $\underset{\sim}{J}_c^{+}$ is the surface current induced on the external side of S_c and J_c^{-}

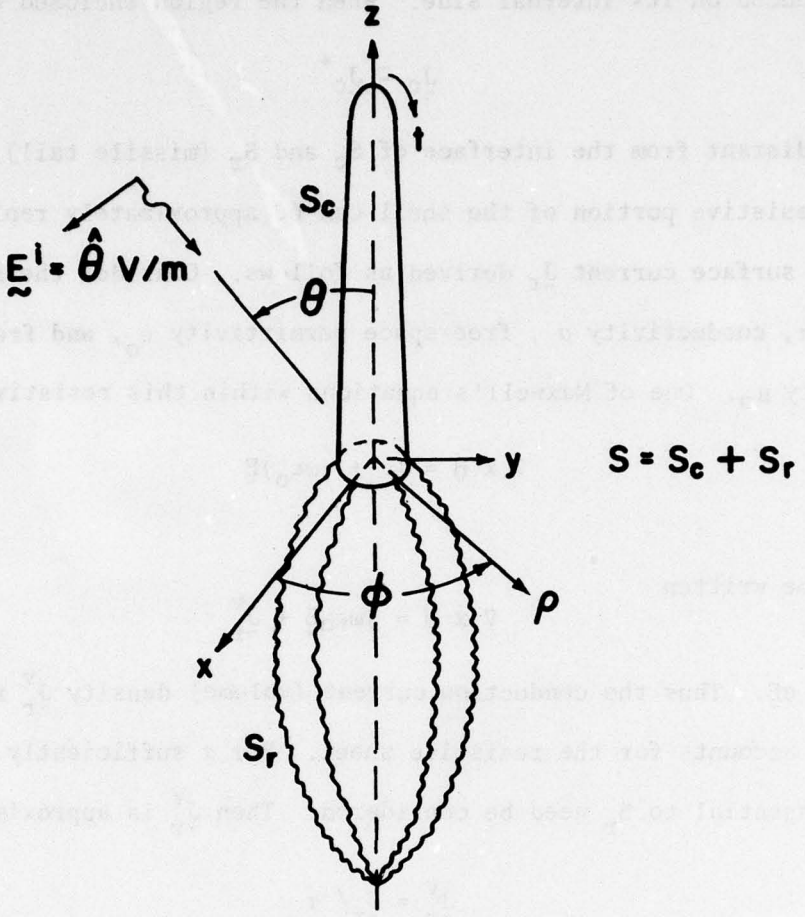

Figure 1. Body of revolution with rotationally symmetric load.

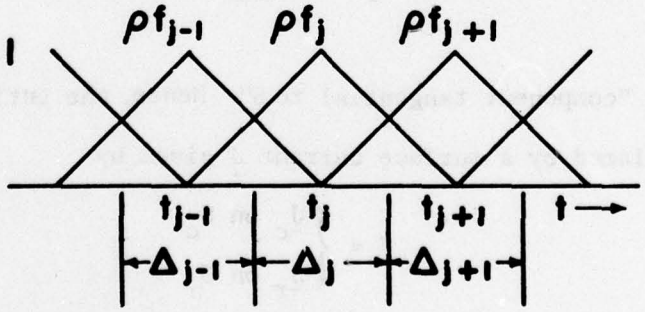

Figure 2. Overlapping triangle expansion functions along generating curve.

is that induced on its internal side. When the region enclosed by S_c is long and thin

$$\underset{\sim}{J}_c \simeq \underset{\sim}{J}_c^+ \tag{2}$$

at points distant from the interface of S_c and S_r (missile tail).

The resistive portion of the shell can be approximately replaced by an equivalent surface current $\underset{\sim}{J}_r$ derived as follows. Consider the sheet to have thickness τ, conductivity σ , free-space permittivity ε_o, and free space permeability μ_o. One of Maxwell's equations within this resistive region is

$$\nabla \times \underset{\sim}{H} = (\sigma + j\omega\varepsilon_o)\underset{\sim}{E} \tag{3}$$

which may be written

$$\nabla \times \underset{\sim}{H} = j\omega\varepsilon_o\underset{\sim}{E} + \underset{\sim}{J}_r^v \tag{4}$$

where $\underset{\sim}{J}_r^v = \sigma\underset{\sim}{E}$. Thus the conduction current (volume) density $\underset{\sim}{J}_r^v$ radiating in free space accounts for the resistive sheet. For τ sufficiently small only the $\underset{\sim}{J}_r^v$ tangential to S_r need be considered. Then $\underset{\sim}{J}_r^v$ is approximated by

$$\underset{\sim}{J}_r^v = \underset{\sim}{J}_r / \tau$$

where

$$\underset{\sim}{J}_r = \sigma\tau\underset{\sim}{E}_{tan} \tag{5}$$

and "tan" denotes "component tangential to S". Hence, the entire shell may be approximately replaced by a surface current $\underset{\sim}{J}$ given by

$$\underset{\sim}{J} = \begin{cases} \underset{\sim}{J}_c \text{ on } S_c \\ \underset{\sim}{J}_r \text{ on } S_r \end{cases}$$

E-field formulations relating $\underset{\sim}{J}$ to $\underset{\sim}{E}_{tan}$ result from

$$\underset{\sim}{E}_{tan} = \underset{\sim}{E}^{i}_{tan} + \underset{\sim}{E}^{s}_{tan}$$

where $\underset{\sim}{E}^{i}$ is the impressed field (body absent) and $\underset{\sim}{E}^{s}$ is the field radiated by $\underset{\sim}{J}$. One such formulation is

$$\underset{\sim}{E}^{i}_{tan} = L(\underset{\sim}{J}) + L^{r}(\underset{\sim}{J}) \tag{6}$$

where

$$L(\underset{\sim}{J}) = -\underset{\sim}{E}^{s}_{tan} = \left[j\omega\mu_o \iint_S \underset{\sim}{J} \frac{e^{-jkR}}{4\pi R} ds + \nabla \frac{j}{\omega\varepsilon_o} \iint_S (\nabla\cdot\underset{\sim}{J}) \frac{e^{-jkR}}{4\pi R} ds \right]_{tan} \tag{7}$$

and $L^{r}(\underset{\sim}{J}) = \underset{\sim}{E}_{tan}$, the loading term, is given by

$$L^{r}(\underset{\sim}{J}) = \begin{cases} 0 & \underset{\sim}{J} = \underset{\sim}{J}_c \\ \frac{1}{\sigma\tau}\underset{\sim}{J} & \underset{\sim}{J} = \underset{\sim}{J}_r \end{cases} \tag{8}$$

In (7) R is the distance between source and field points on S, the integrations are with respect to the source points, and the remaining symbols have their usual meanings.

An approximation to $\underset{\sim}{J}$ satisfying (6) can be found by moment methods. Consider the coordinate system of Figure 1. A set of expansion functions $\underset{\sim}{F}^{t}_{nj} = f_j(t)e^{jn\phi}\hat{t}$ and $\underset{\sim}{F}^{\phi}_{nj} = f_j(t)e^{jn\phi}\hat{\phi}$ ($\hat{t}$ and $\hat{\phi}$ are unit vectors) and the symmetric product

$$< J_1, J_2 > = \iint_S \underset{\sim}{J}_1 \cdot \underset{\sim}{J}_2 \, ds = \int_{gc}\int_0^{2\pi} \underset{\sim}{J}_1 \cdot \underset{\sim}{J}_2 \, \rho d\phi dt$$

are chosen where the "gc" stands for "BOR generating curve". (The generating curve is a line in any plane containing the BOR axis which, when

revolved around this axis, traces out a surface enclosing the BOR). The $f_j(t)$, which express the t variation of the expansion functions, are usually selected in accordance with the method of subsections [5]. In the Harrington-Mautz method they are unit triangles (overlapping) divided by the BOR surface radial coordinate (Figure 2). This choice permits differentiation of the expansion functions and a non-zero value where the poles of the BOR meet the axis. The $e^{jn\phi}$ are chosen to invoke the modal decoupling property of rotationally symmetric bodies. Thus for M triangles on the generating curve $\underset{\sim}{J}$ is expanded as

$$\underset{\sim}{J} = \sum_{n=-\infty}^{\infty} \sum_{j=1}^{M} (I_{nj}^{t} f_j(t) e^{jn\phi} \hat{t} + I_{nj}^{\phi} f_j(t) e^{jn\phi} \hat{\phi}) \tag{9}$$

where I_{nj}^{t} and I_{nj}^{ϕ} are the unknown coefficients to be determined such that (6) is satisfied. The inner products of both sides of (6) are taken with respect to each of the weighting functions $\underset{\sim}{W}_{ni}^{t} = f_i(t) e^{-jn\phi} \hat{t}$ and $W_{ni}^{\phi} = f_i(t) e^{-jn\phi} \hat{\phi}$ resulting in the matrix equation

$$\vec{V}_n = [Z_n] \vec{I}_n \tag{10}$$

for each mode n. Upon partitioning, (10) becomes

$$\begin{bmatrix} V_n^t \\ \hline V_n^{\phi} \end{bmatrix} = \left[\begin{array}{c|c} [Z_n^{tt}] & [Z_n^{t\phi}] \\ \hline [Z_n^{\phi t}] & [Z_n^{\phi\phi}] \end{array}\right] \begin{bmatrix} \vec{I}_n^t \\ \hline \vec{I}_n^{\phi} \end{bmatrix}$$

The i^{th} element of each $\vec{V}_n^a$ and $\vec{I}_n^a$ subvector (a=t or a=ϕ) is $\langle W_{ni}^a , E^i \rangle$ and I_{ni}^a respectively, and the i, j^{th} element of each $[Z_n^{ab}]$ submatrix is

$< W^a_{ni}, LF^b_{nj} > + < W^a_{ni}, L^r F^b_{nj} >$ where ab takes on the combinations tt, ϕt, tϕ, $\phi\phi$. The computation of $< W^a_{ni}, LF^a_{nj} >$ is detailed in [1,2]. Computation of $< W^a_{ni}, L^r F^b_{nj} >$ is simplified by first approximating the distributed resistance $\frac{1}{\sigma\tau}$ along S_r with infinitely thin load rings. Each ring is located at the "peak", $t=t_j$ in Figure 2, of an $f_j(t)$ on S_r. Thus

$$\frac{1}{\sigma\tau} \approx \sum_j \frac{\Delta_j}{\sigma_j \tau_j} \delta(t-t_j) \quad t \text{ on } S_r$$

where each $\sigma_j\tau_j$ is evaluated at $t=t_j$, the segment lengths Δ_j are defined in Figure 2, and $\delta(t)$ is the unit impulse function. Therefore, for all j such that t_j is on S_c

$$< W^t_{ni}, L^r F^t_{nj} > = < W^\phi_{ni}, L^r F^\phi_{nj} > = 0$$

and for all j such that t_j is on S_r

$$< W^t_{ni}, L^r F^t_{nj} > = < W^\phi_{ni}, L^r F^\phi_{nj} > = \begin{cases} \frac{2\pi\ \Delta_j}{\sigma_j \tau_j \rho_j} & i=j \\ 0 & i \neq j \end{cases}$$

where ρ_j is the radius of the BOR surface at t_j. Also,

$$< W^t_{ni}, L^r F^\phi_{nj} > = < W^\phi_{ni}, L^r F^t_{nj} > = 0$$

Thus the loading affects only the diagonal elements of $[Z_n]$.

Each mode of $\underset{\sim}{J}$ is determined independently from (9, 10) resulting in significant savings in computer processing time and memory. The solution to (10) can be expressed as

$$\vec{I}_n = [Y_n]\ \vec{V}_n \tag{11}$$

where $[Y_n] = [Z_n]^{-1}$ is the generalized admittance matrix.

3. Model

The missile body was modeled as a perfectly conducting cylindrical shell of length = 1.22m and diameter = 0.05m. Its BOR generating curve is the $z>0$ portion of the contour shown in Figure 3. The cylinder is closed at one end (missile nose) and open at the other (missile tail or thruster). For the results presented in the following section the cylinder was lengthened an additional 0.1m. This was to reflect the presence of tail fins extending beyond the missile thrust orifice.

An equivalent sheet admittance $y=\sigma\tau$ and radius ρ_e for the plume portion of the model was derived from recently available plume constituent data [6,8]. The latter was obtained from a theoretical analysis employing the known chemical composition of the missile fuel. The plume's permittivity and permeability were found to be essentially free-space values. Thus only plume conductivity data was considered in development of the model. The y and ρ_e were determined by first extracting from this data, for each of a number of plume axial positions, the peak conductivity σ_m its radial coordinate ρ_m and the additional outward radial distance to the point of 10% fall-off from σ_m, $\Delta\rho$. These parameters are tabulated in Table I. A conductivity profile, between $0.1\sigma_m$ points, for a typical plume cross-section is shown in Figure 4.

Reasonable values of y and ρ_e were then chosen by assuming (a) $\sigma=0$ for $\rho<\rho_m$, (b) a linear conductivity decay from σ_m at ρ_m to zero at $\rho_m+\Delta\rho$ as depicted by the dashed line in Figure 4, (c) the admittance y is equal to the area under this assumed curve and (d) y is lumped into the edge of a circle with radius $\rho_m+\Delta\rho/2$. Thus

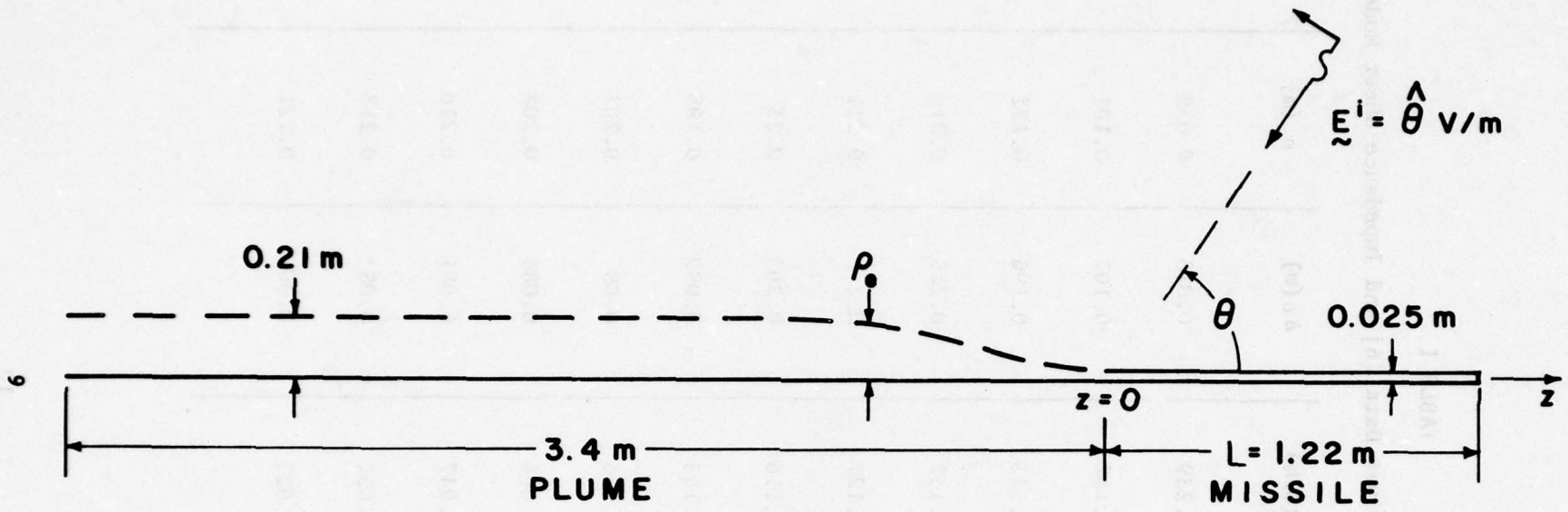

Figure 3. Body of revolution generating curve (to scale) for model of missile with plume.

TABLE I

Characteristics of Plume Data [6] and Impedance Sheet Model

z(m)	ρ_m(m)	σ_m(S/m)	$\Delta\rho$(m)	ρ_e(m)	y(mS)
-0.1	0.023	0.239	0.013	0.030	1.55
-0.38	0.047	0.162	0.107	0.101	8.67
-0.69	0.074	0.143	0.196	0.172	14.0
-0.99	0.103	0.132	0.225	0.216	14.9
-1.14	0.111	0.127	0.2	0.211	12.9
-1.44	0.128	0.116	0.203	0.23	11.8
-1.75	0.145	0.103	0.099	0.195	5.1
-2.05	0.163	0.086	0.08	0.203	3.44
-2.36	0.166	0.066	0.084	0.208	2.77
-2.67	0.169	0.047	0.081	0.210	7.61
-3.01	0.173	0.032	0.08	0.213	1.28
-3.32	0.176	0.022	0.09	0.221	0.99

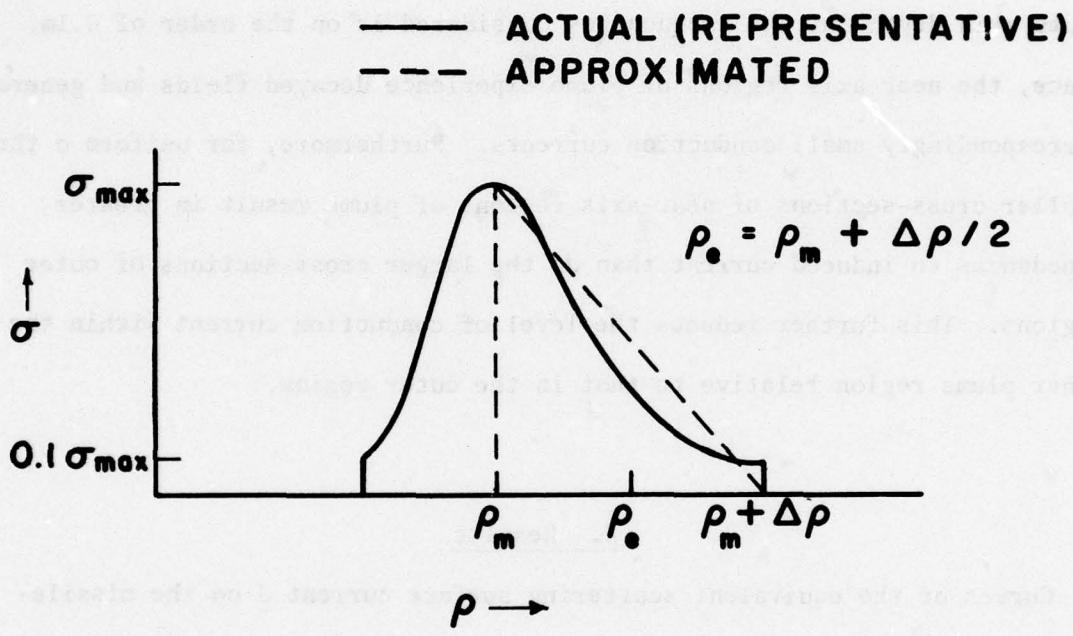

Figure 4. Conductivity profile, between points of 10% peak conductivity, for a typical plume cross-section.

$$y=\sigma_m \Delta\rho/2$$

$$\rho_e=\rho_m+\Delta\rho/2$$

Numerical values of y and ρ_e are also given in Table I.

The justification for assumption (a) above is based on the following: Plume skin depth for the frequencies considered is on the order of 0.1m. Hence, the near-axis regions of plume experience decayed fields and generate correspondingly small conduction currents. Furthermore, for uniform σ the smaller cross-sections of near-axis regions of plume result in greater impedances to induced current than do the larger cross-sections of outer regions. This further reduces the level of conduction current within the inner plume region relative to that in the outer region.

4. Results

Curves of the equivalent scattering surface current $\underset{\sim}{J}$ on the missile-plus-plume model discussed above are presented in this section. The incident field is a θ-polarized unit plane wave (Figures 1, 3). Accompanying each curve is a corresponding plume-absent result thus permitting direct evaluation of the plume effect on missile skin current. Results are given for broadside excitation ($\theta=90°$) at frequencies from 25 MHz to 275 MHz for which the cylinder (missile) length varies electrically from ~0.1λ to ~1.1λ. Included also are results for oblique incidence excitation ($15° \leq \theta \leq 165°$) at frequencies of 25 MHz, 100 MHz, and 250 MHz.

Only the circumferentially uniform (n=0) $\underset{\sim}{J}$ mode is considered. Since $\underset{\sim}{E}^i$ is θ-polarized, the ϕ-directed component of $\underset{\sim}{J}$ for this mode is zero [1,2]. Circumferentially non-uniform modes ($n \geq 1$) are not considered, since for thin bodies these modal components of missile current $\underset{\sim}{J}_c$ are not influenced significantly by plume presence. This is because the z-directed components of the non-uniform $\underset{\sim}{J}$ modes for fairly thin bodies are colinearly weakly coupled and for θ-polarized excitation their ϕ-directed components are small [7]. This does not infer, however, that the principal (n=1) non-uniform current mode is insignificant. In fact it has been found to be on the order of 70% that of the uniform mode for wavelength long cylinders with less than 0.1λ diameters [7]. Furthermore, under axial incidence excitation only the n=1 mode is excited [1,2]. Thus the oblique incidence excitation examples are limited to $15^\circ \leq \theta \leq 165^\circ$.

The number of expansion functions chosen for all runs was M=50. This choice resulted in reasonable current magnitude precision for frequencies up to 275 MHz.

The plume-absent results are approximations obtained by replacing the values of equivalent sheet admittance representing the plume (y in Table I) with $y=10^{-5}$S. This model was used instead of an "actual" plume-absent model (model only the cylindrical representation of the missile) since it demonstrated validity of the lumped load approximation described in Section 2. As will be apparent in all examples, the plume current on the approximate plume-absent model is insignificant. Approximate plume-absent results were also compared with "actual" plume-absent results for a few cases with the resulting missile current being indistinguishable.

Predictions of outside surface skin current very near the missile tail are not reliable. This is due, in part, to the over-simplified model of the complicated thrust orifice region. Also, at locations extremely close to the orifice, (within a length equal to the missile diameter) (2) is not valid.

As mentioned previously tail fins on the actual missile extend beyond the orifice region toward the plume. Thus the conducting cylinder representing the missile was extended 0.1m. That explains why the current drops to zero 0.1m beyond the orifice plane (z=0) in all plume-absent results.

4.1 Broadside Excitation

In Figures 5-15 current magnitude $|\underset{\sim}{J}|$, is plotted in dB for broadside excitation ($\theta=90^{\circ}$) and for frequencies from 25 MHz to 275 MHz at 25 MHz intervals. At 25 MHz the missile length L is approximately 0.1λ.
As indicated in Figure 5, the plume introduces a "lengthening" effect not unlike that from capacitively loading a short dipole. Thus, as expected, the "missile" current $|\underset{\sim}{J}_c|$, especially near the tail, is significantly enhanced by the plume. The apparent discontinuity in $|\underset{\sim}{J}|$ at the missile-plume interface occurs because $\underset{\sim}{J}$ is a surface current density and plume radius ρ_e increases rapidly away from this plane. The total current $2\pi\rho_e|\underset{\sim}{J}|$ varies more smoothly.

The only other significant plume effect, for broadside incidence, (at missile surface locations other than the orifice) occurs at 100 MHz where the unloaded missile is near resonance ($L/\lambda \approx 0.4$). In Figure 8 a 7 dB reduction in $|\underset{\sim}{J}_c|$ due to the plume indicates that the plume now acts as a detuning load.

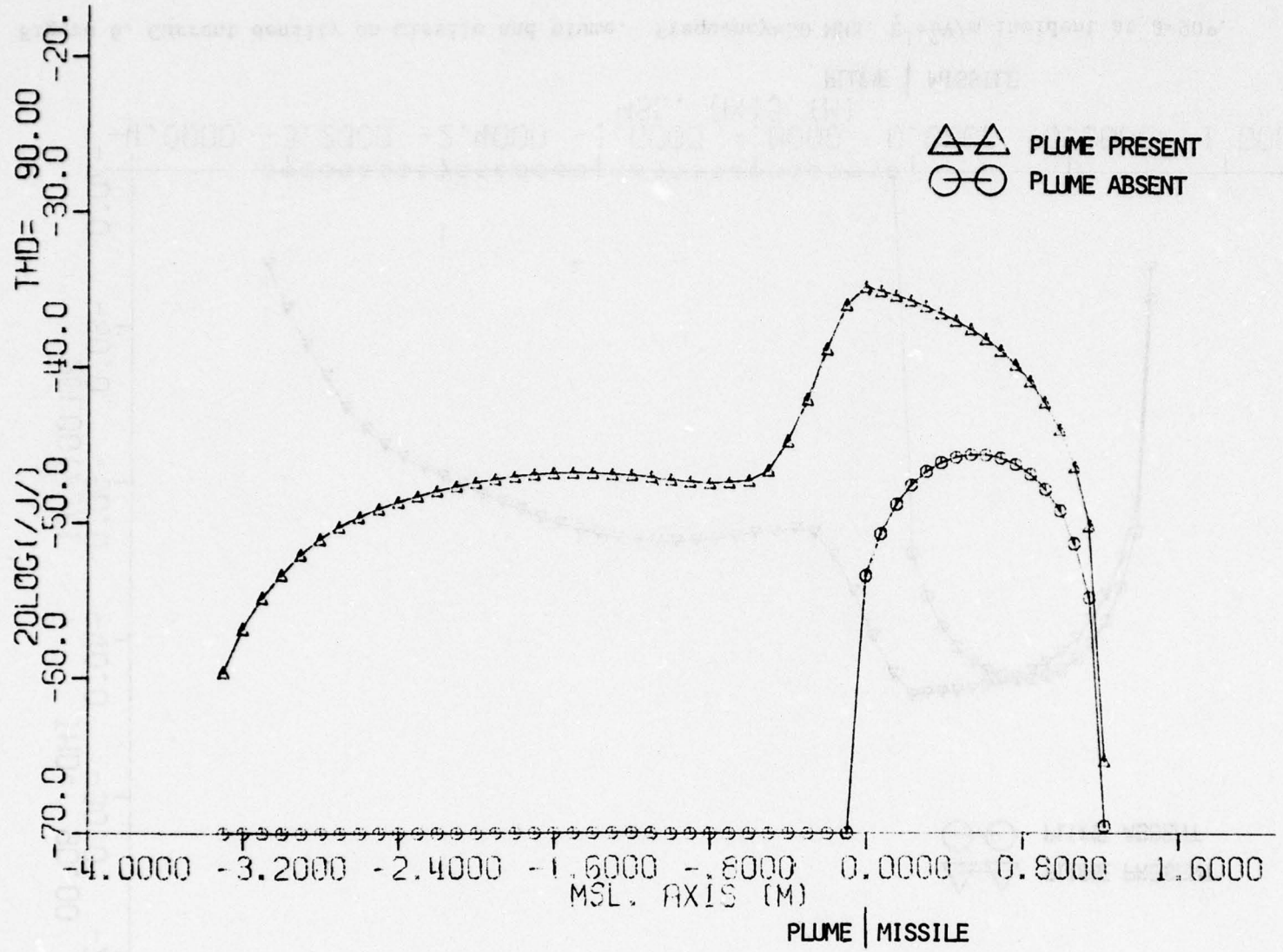

Figure 5. Current density on missile and plume. Frequency = 25 MHz. $\underline{E}^i = \hat{\theta}$V/m incident at $\theta=90°$.

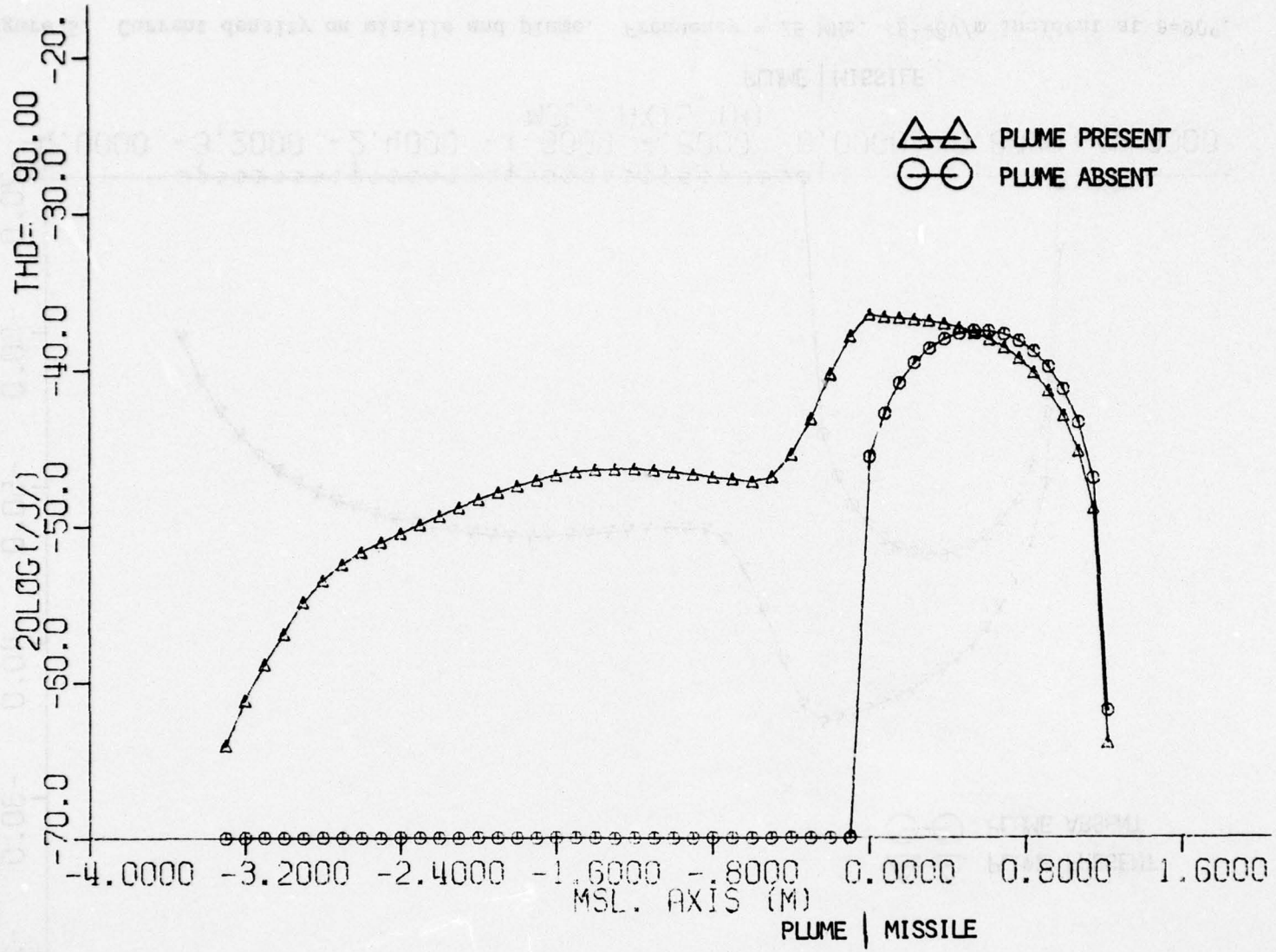

Figure 6. Current density on missile and plume. Frequency=50 MHz. $\underset{\sim}{E}^{i}=\hat{\theta}$V/m incident at $\theta=90°$.

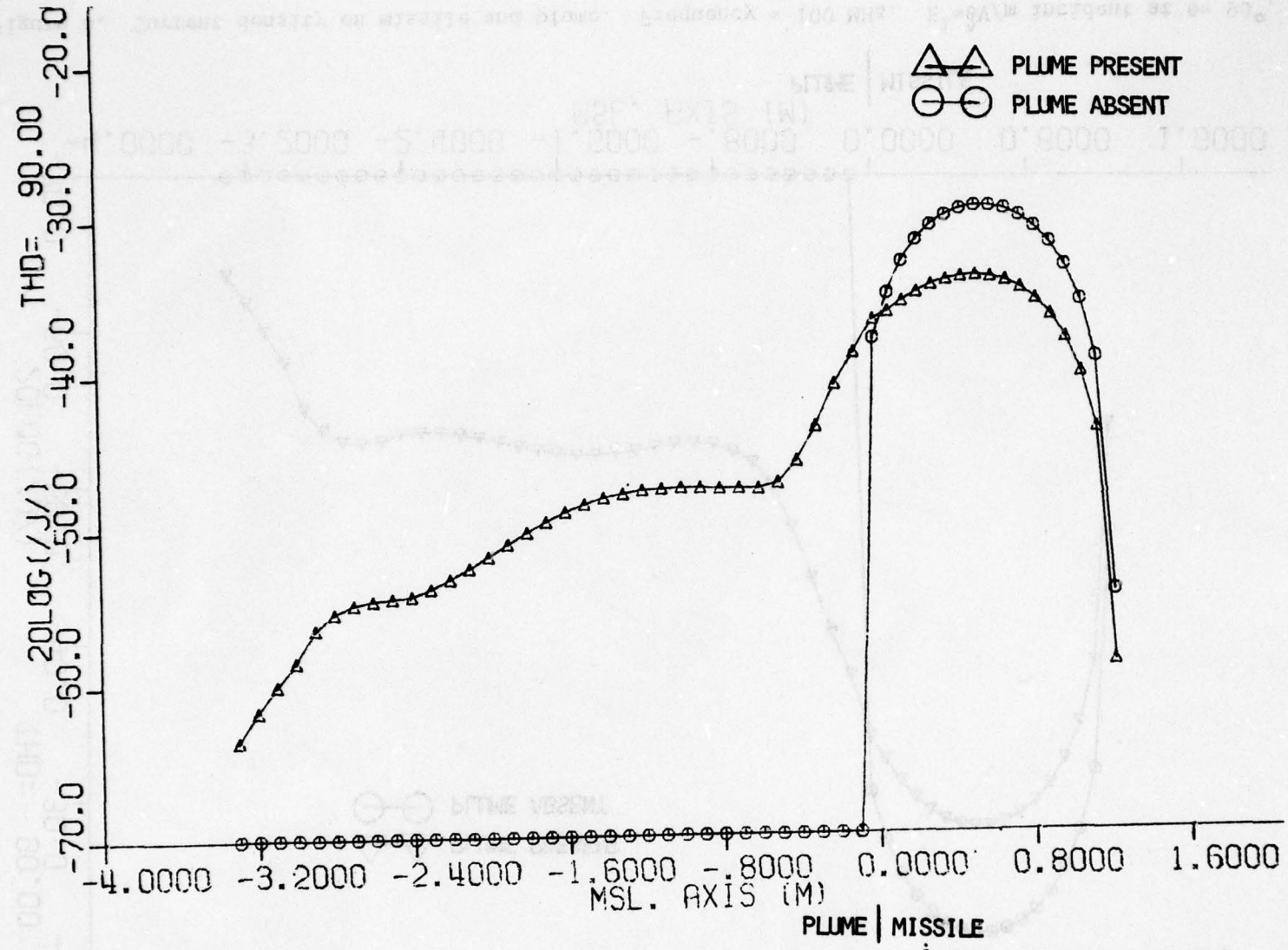

Figure 7. Current density on missile and plume. Frequency = 75 MHz: $\underset{\sim}{E}^{i}=\hat{\theta}$V/m incident at $\theta=90^{c}$.

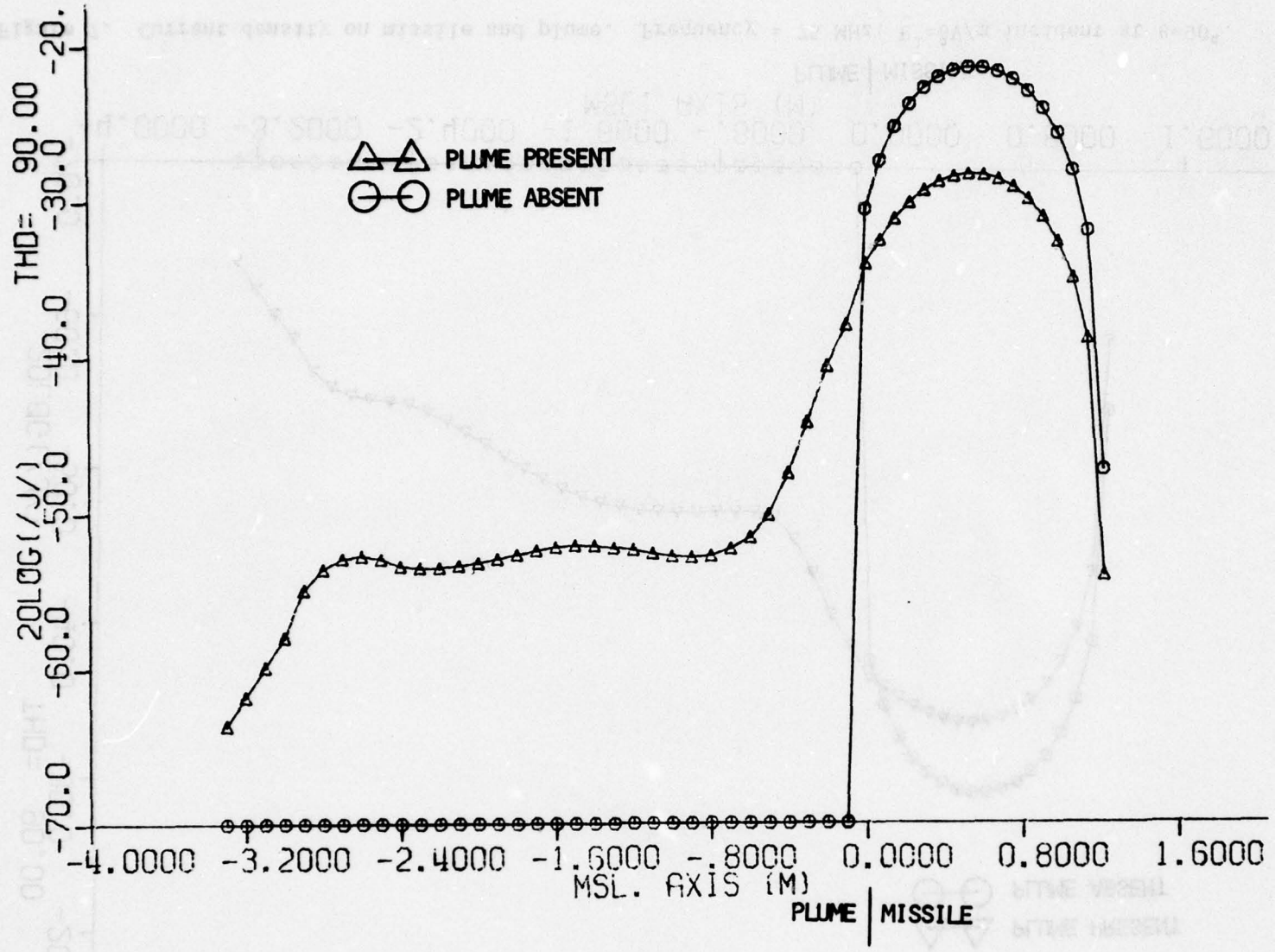

Figure 8. Current density on missile and plume. Frequency = 100 MHz. $\underset{\sim}{E}^{i}=\hat{\theta}$V/m incident at $\theta= 90^{\circ}$.

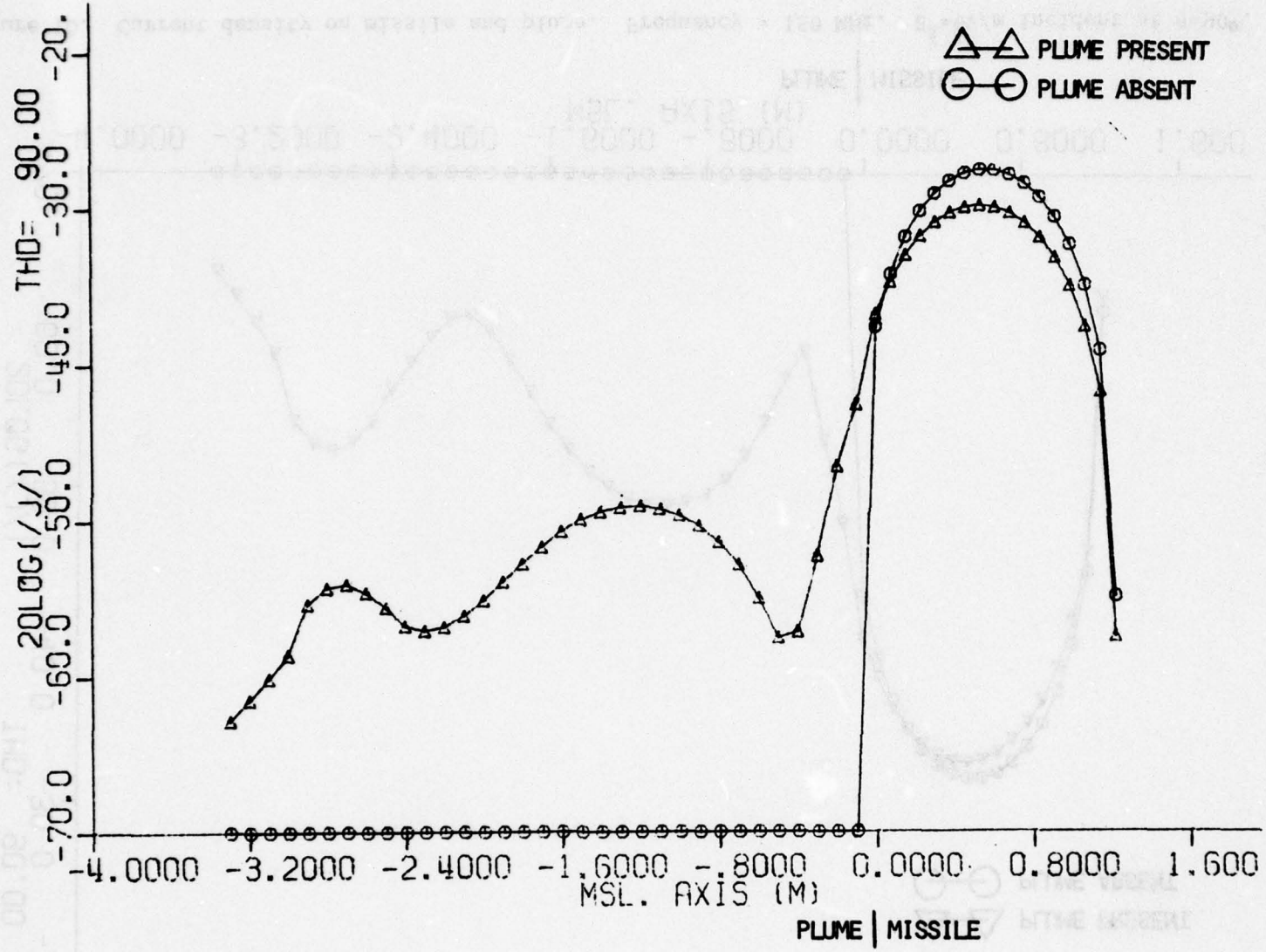

Figure 9. Current density on missile and plume. Frequency = 125 MHz. $\underset{\sim}{E}^{i}=\hat{\theta}$V/m incident at $\theta=90^{\bullet}$.

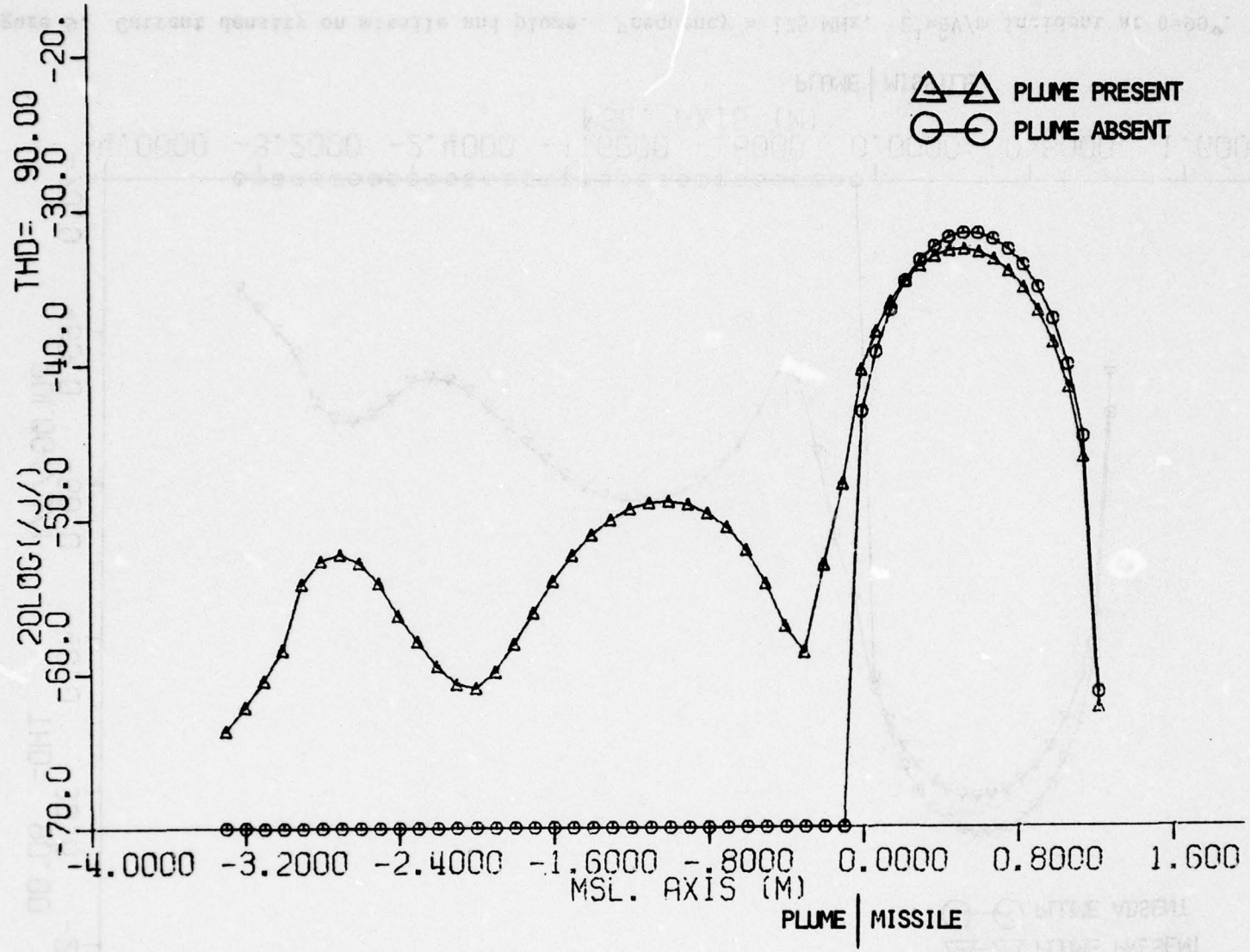

Figure 10. Current density on missile and plume. Frequency = 150 MHz. $\underset{\sim}{E}^{i}=\hat{\theta}$V/m incident at $\theta=90^{\circ}$.

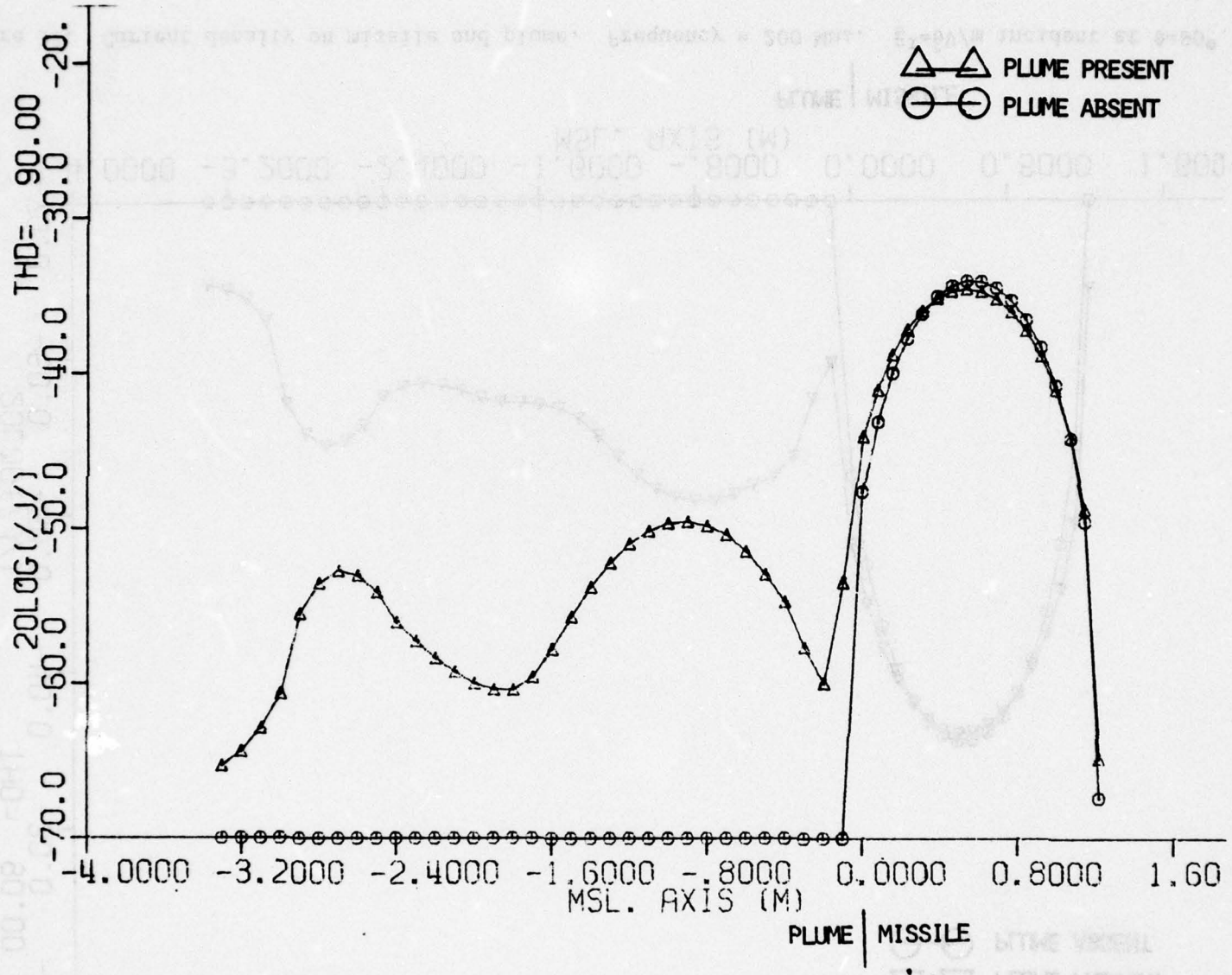

Figure 11. Current density on missile and plume. Frequency = 175 MHz. $\tilde{E}^i = \hat{\theta}$V/m incident at $\theta=90^\circ$.

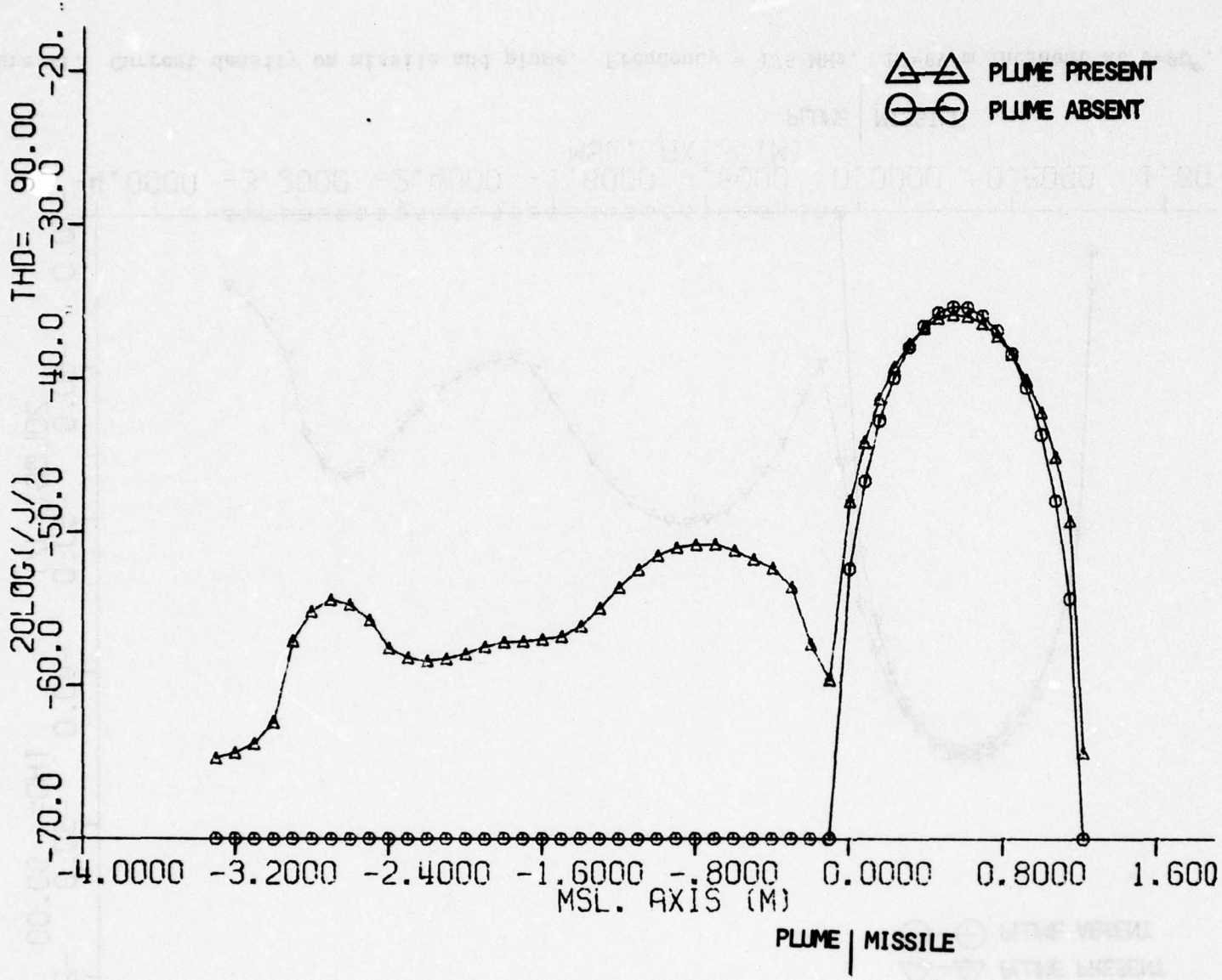

Figure 12. Current density on missile and plume. Frequency = 200 MHz. $\underline{E}^i = \hat{\theta}$V/m incident at $\theta = 90°$.

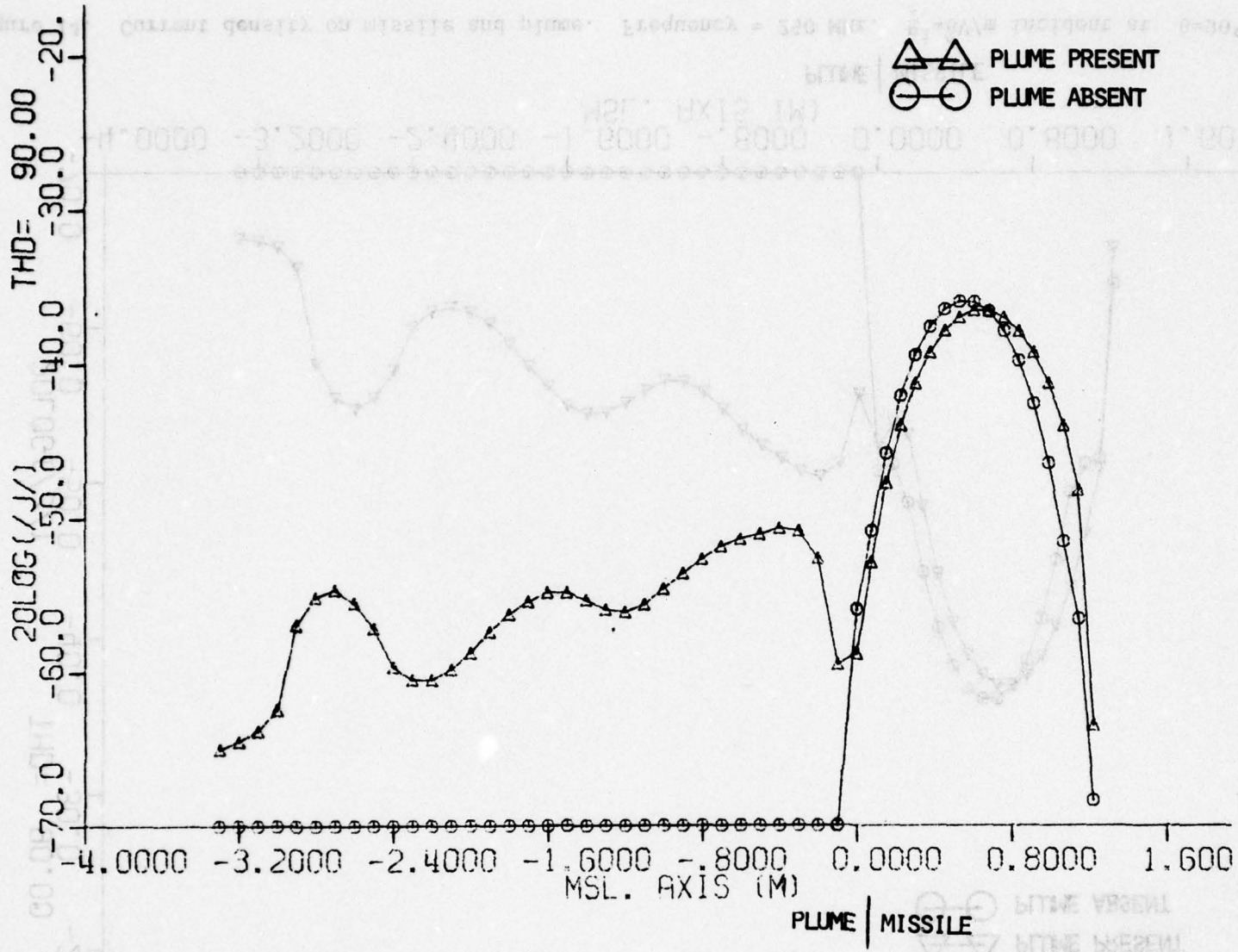

Figure 13. Current density on missile and plume: Frequency = 225 MHz. $\underset{\sim}{E}^{i}=\hat{\theta}$V/m incident at $\theta=90°$.

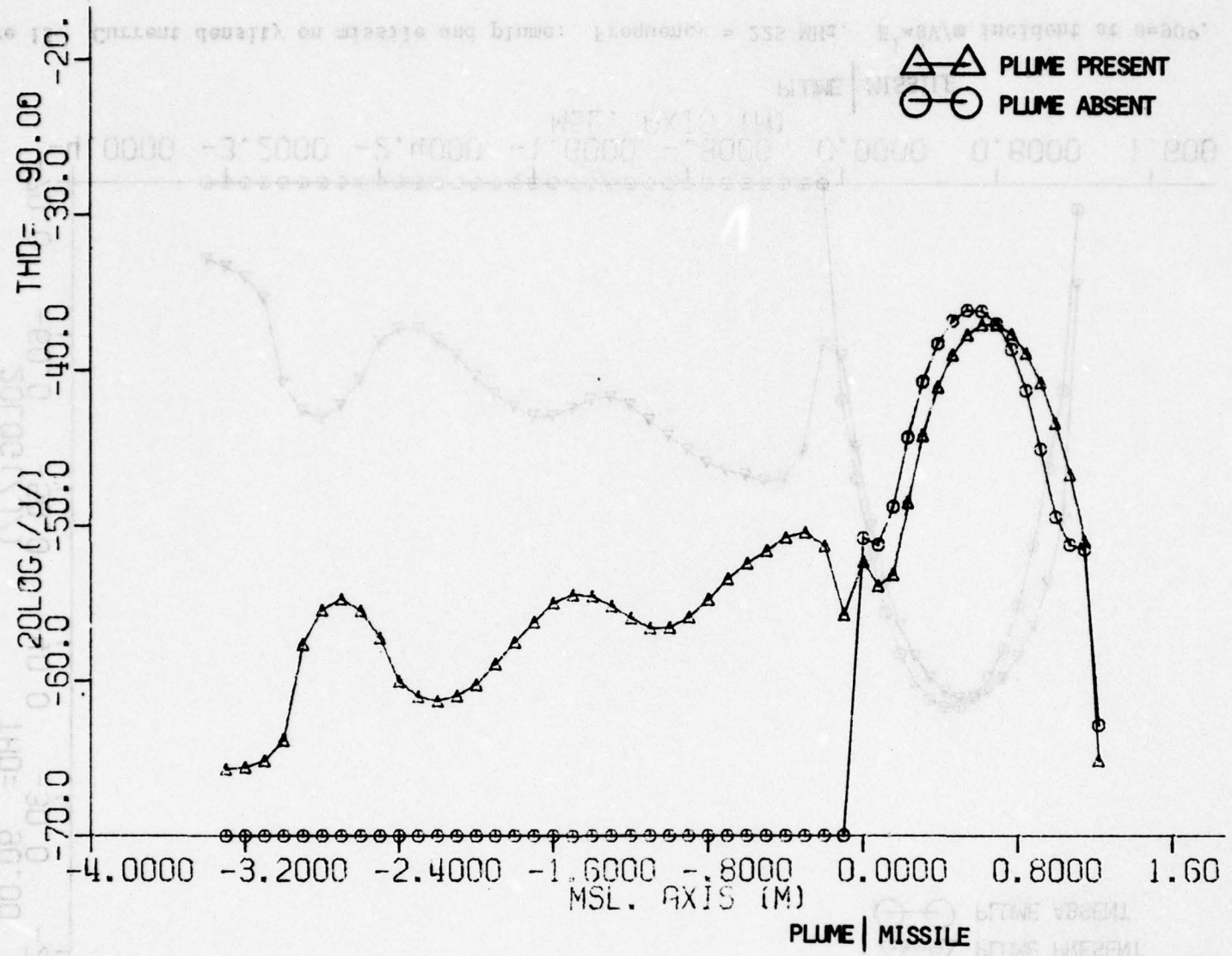

Figure 14. Current density on missile and plume. Frequency = 250 MHz. $\underset{\sim}{E}^{i}=\hat{\theta}$V/m incident at $\theta=90°$.

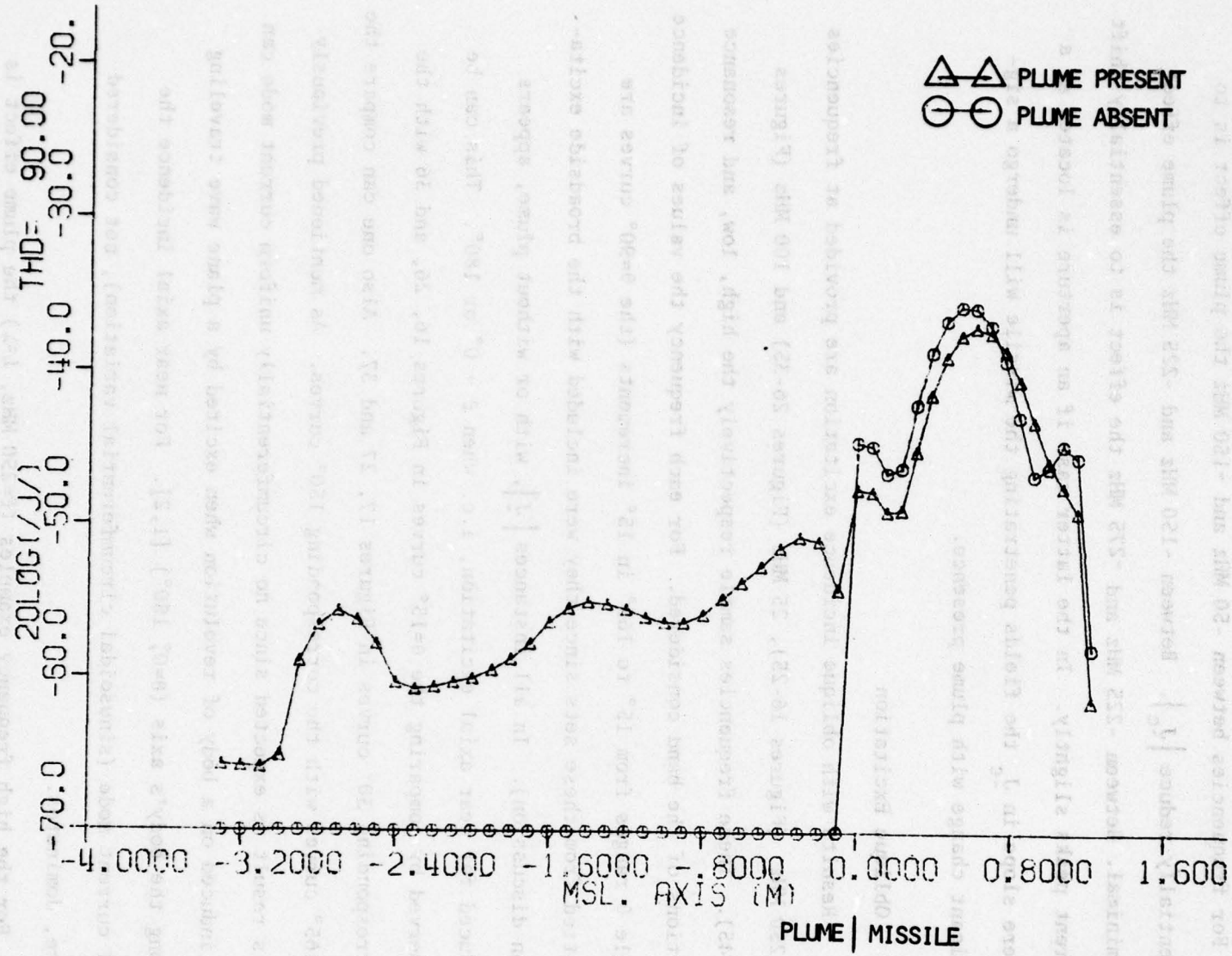

Figure 15. Current density on missile and plume. Frequency = 275 MHz. $\underset{\sim}{E}^{i} = \hat{\theta}$V/m incident at $\theta=90^{\circ}$.

For frequencies between ~50 MHz and ~150 MHz the plume effect is to essentially reduce $|\underset{\sim}{J}_c|$. Between ~150 MHz and ~225 MHz the plume effect is minimal. Between ~225 MHz and ~275 MHz the effect is to essentially shift current peaks slightly. In the latter case if an aperture is located at a severe slope in $\underset{\sim}{J}_c$ the fields penetrating the missile will undergo a significant change with plume presence.

4.2 Oblique Excitation

Results with oblique incidence excitation are provided at frequencies of 250 MHz (Figures 16-25), 25 MHz (Figures 26-35) and 100 MHz (Figures 36-45). These frequencies sample respectively the high, low, and resonance portions of the band considered. For each frequency the values of incidence angle θ ranges from 15° to 165° in 15° increments (the θ=90° curves are omitted from these sets since they were included with the broadside excitation discussion). In all instances $|\underset{\sim}{J}|$, with or without plume, appears reduced for near axial excitation, i.e. when $\theta \rightarrow 0°$ or 180°. This can be observed by comparing the θ=15° curves in Figures 16, 26, and 36 with the corresponding 30° curves in Figures 17, 27 and 37. Also one can compare the θ=165° curves with the corresponding 150° curves. As mentioned previously this result is expected since no circumferentially uniform current mode can be induced on a body of revolution when excited by a plane wave traveling along the body's axis (θ=0°, 180°) [1,2]. For near axial incidence the n=1 current mode (sinusoidal circumferential variation), not considered here, dominates.

For the high frequency examples (f=250 MHz, $L \approx \lambda$) the plume effect is

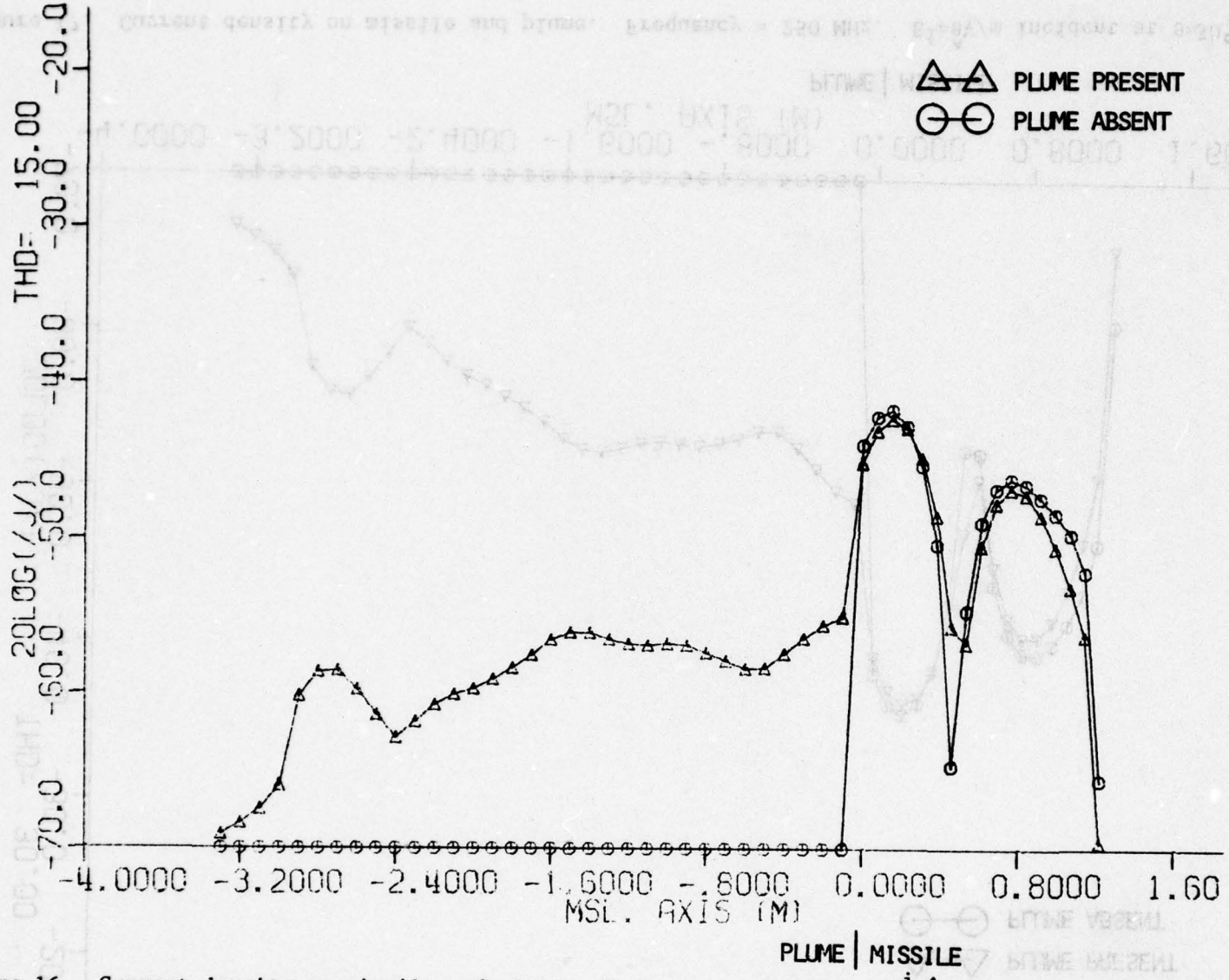

Figure 16. Current density on missile and plume. Frequency = 250 MHz. $\tilde{E}^i = \hat{\theta}$V/m incident at $\theta = 15°$.

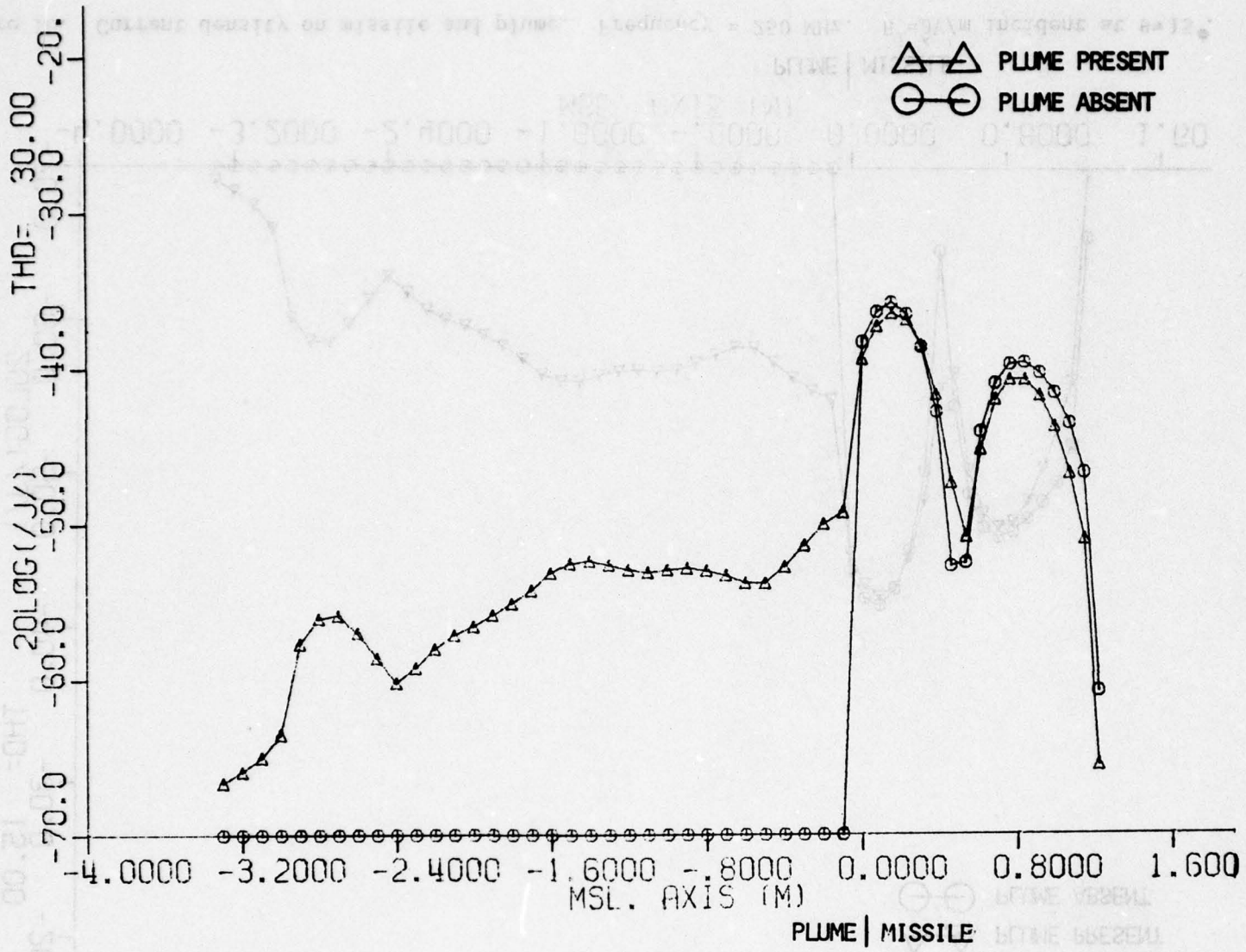

Figure 17. Current density on missile and plume. Frequency = 250 MHz. $E^i = \hat{\theta}$V/m incident at $\theta = 30°$.

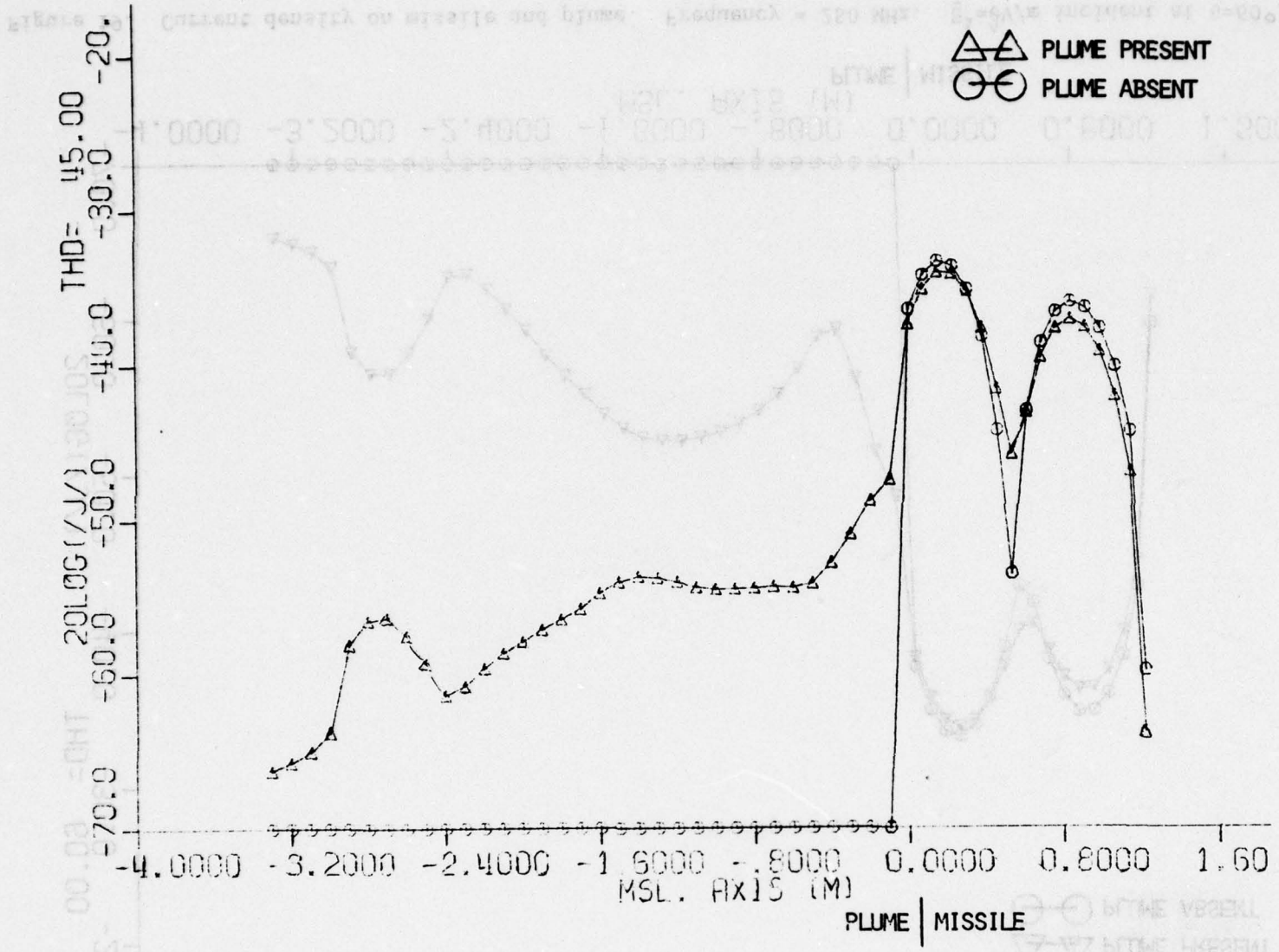

Figure 18. Current density on missile and plume. Frequency = 250 MHz. $\underset{\sim}{E}^{i}=\hat{\theta}$V/m incident at $\theta=45°$.

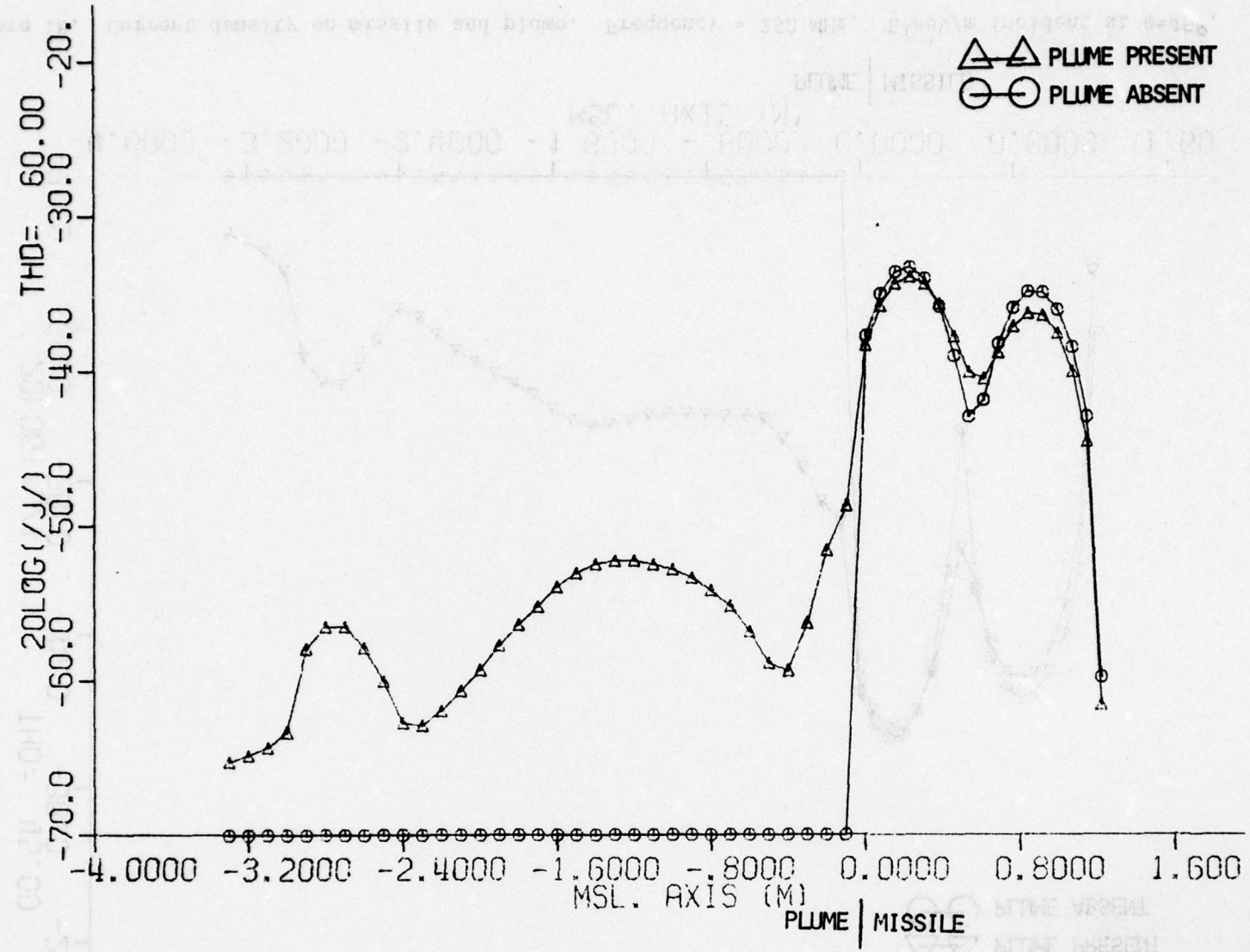

Figure 19. Current density on missile and plume. Frequency = 250 MHz. $\underset{\sim}{E}^{i}=\hat{\theta}$V/m incident at $\theta=60°$.

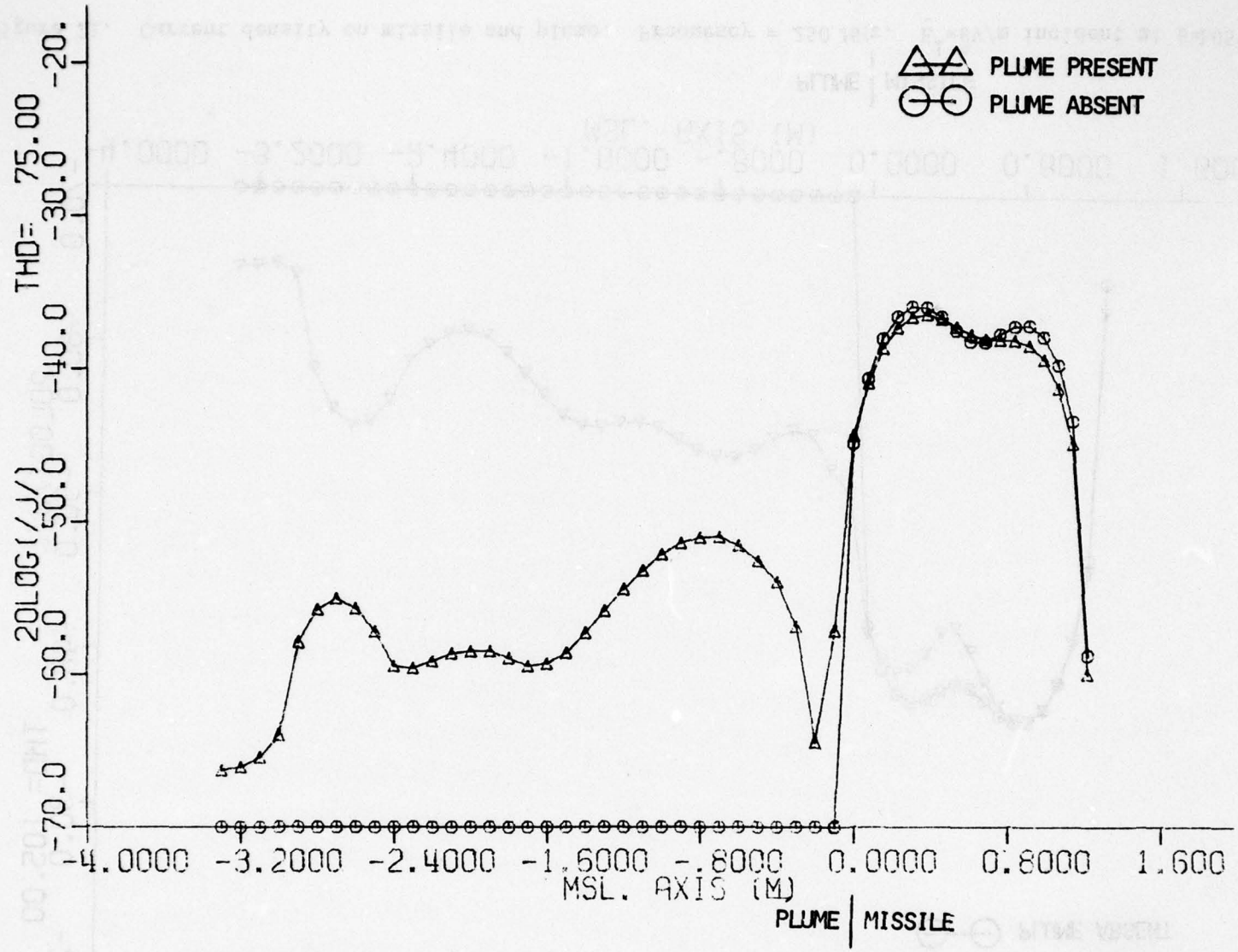

Figure 20. Current density on missile and plume. Frequency = 250 MHz. $\underset{\sim}{E}^{i}=\hat{\theta}$V/m incident at $\theta=75°$.

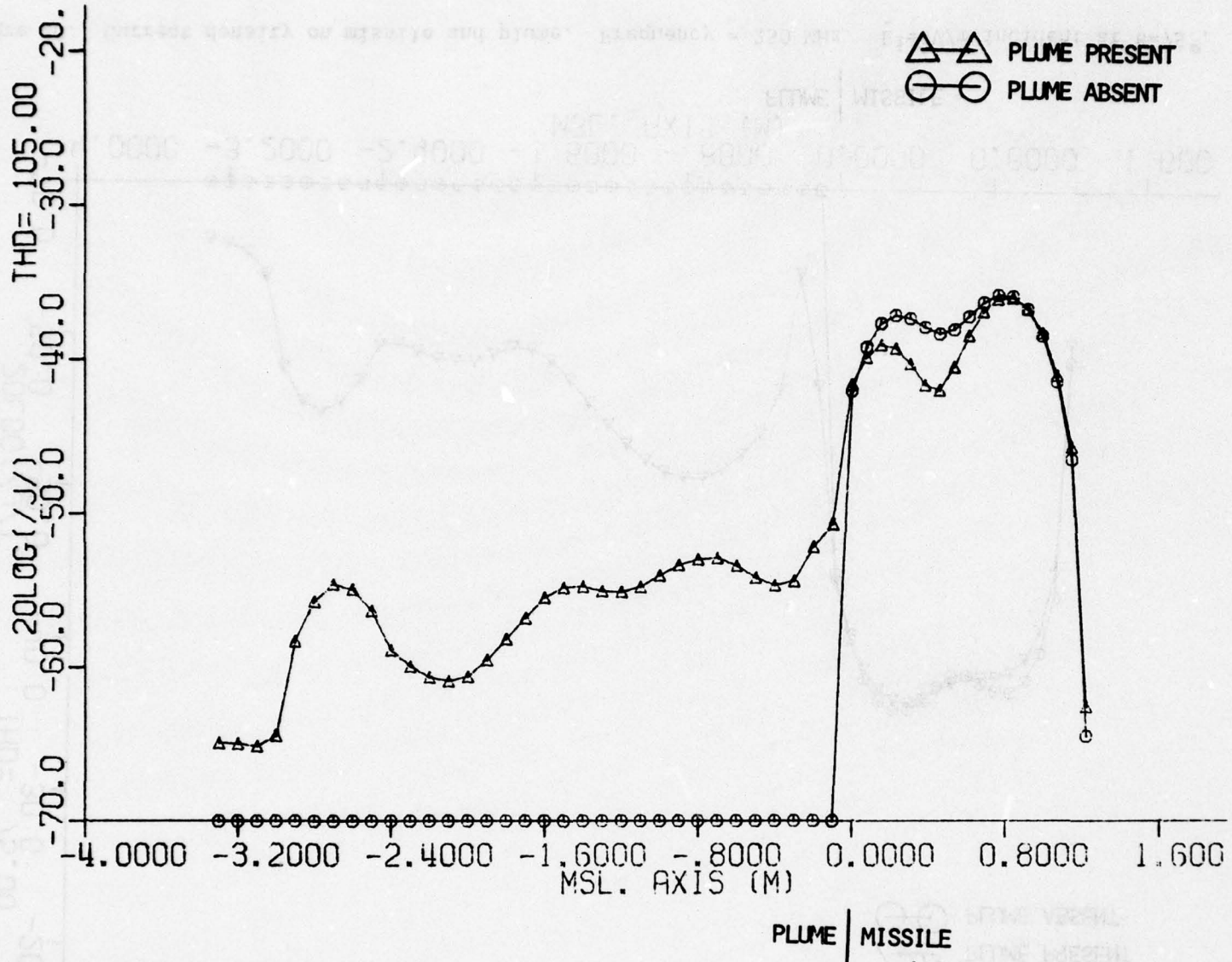

Figure 21. Current density on missile and plume. Frequency = 250 MHz. $\underset{\sim}{E}^{i}=\hat{\theta}$V/m incident at $\theta=105°$.

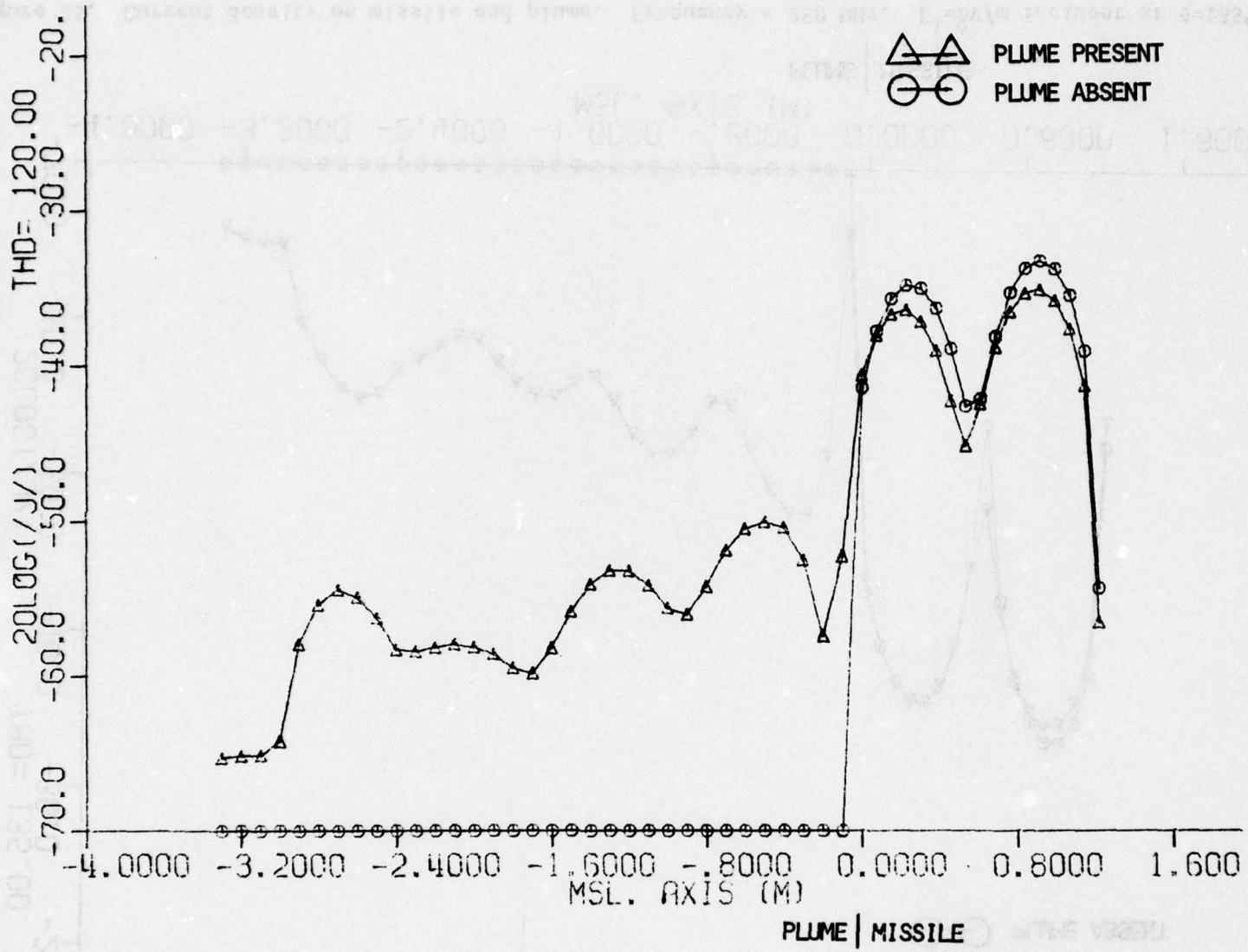

Figure 22. Current density on missile and plume. Frequency = 250 MHz. $\underset{\sim}{E}^{i}=\hat{\theta}$V/m incident at $\theta=120^{\circ}$.

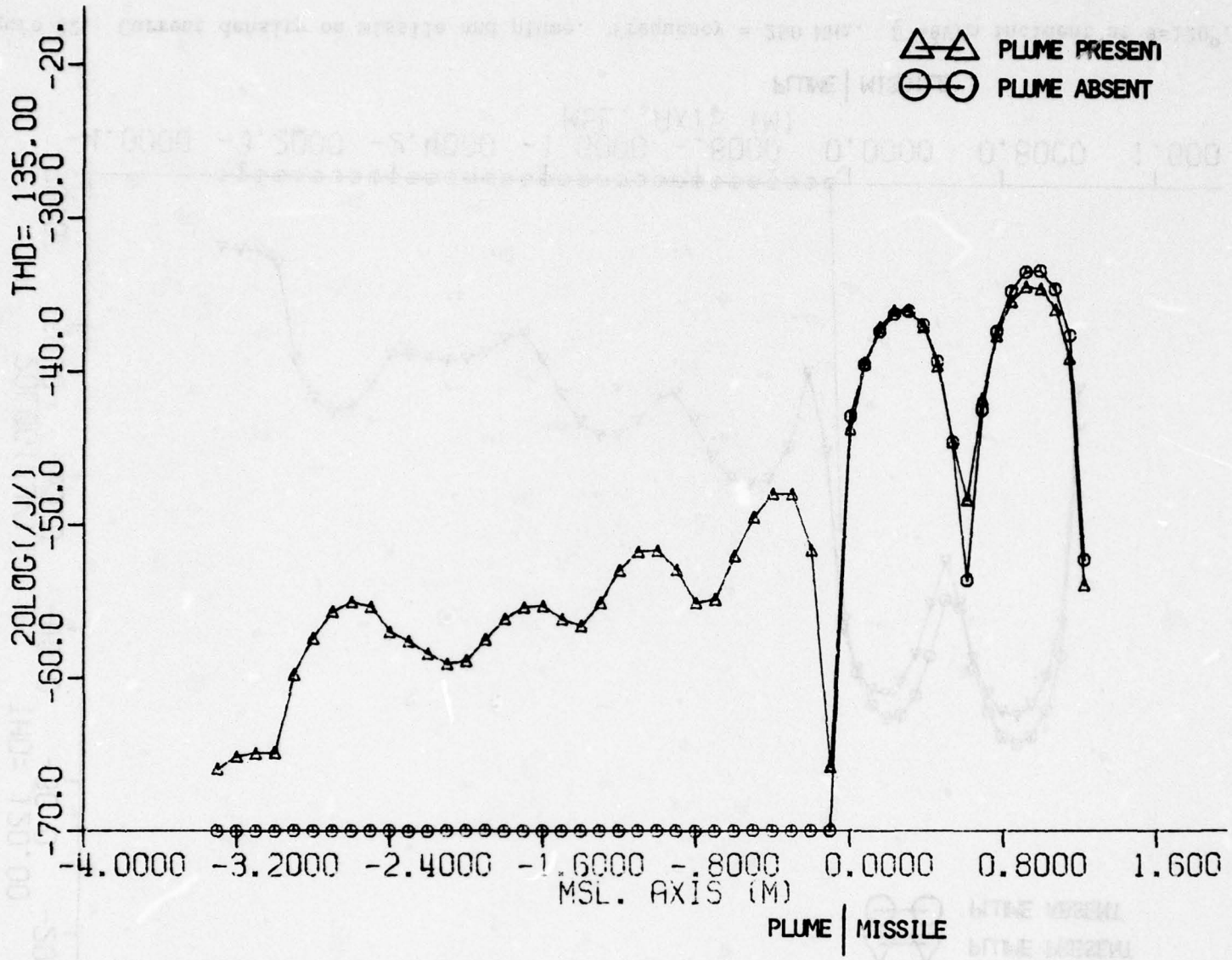

Figure 23. Current density on missile and plume. Frequency = 250 MHz. $\underset{\sim}{E}^{i}=\hat{\theta}$V/m incident at $\theta=135°$.

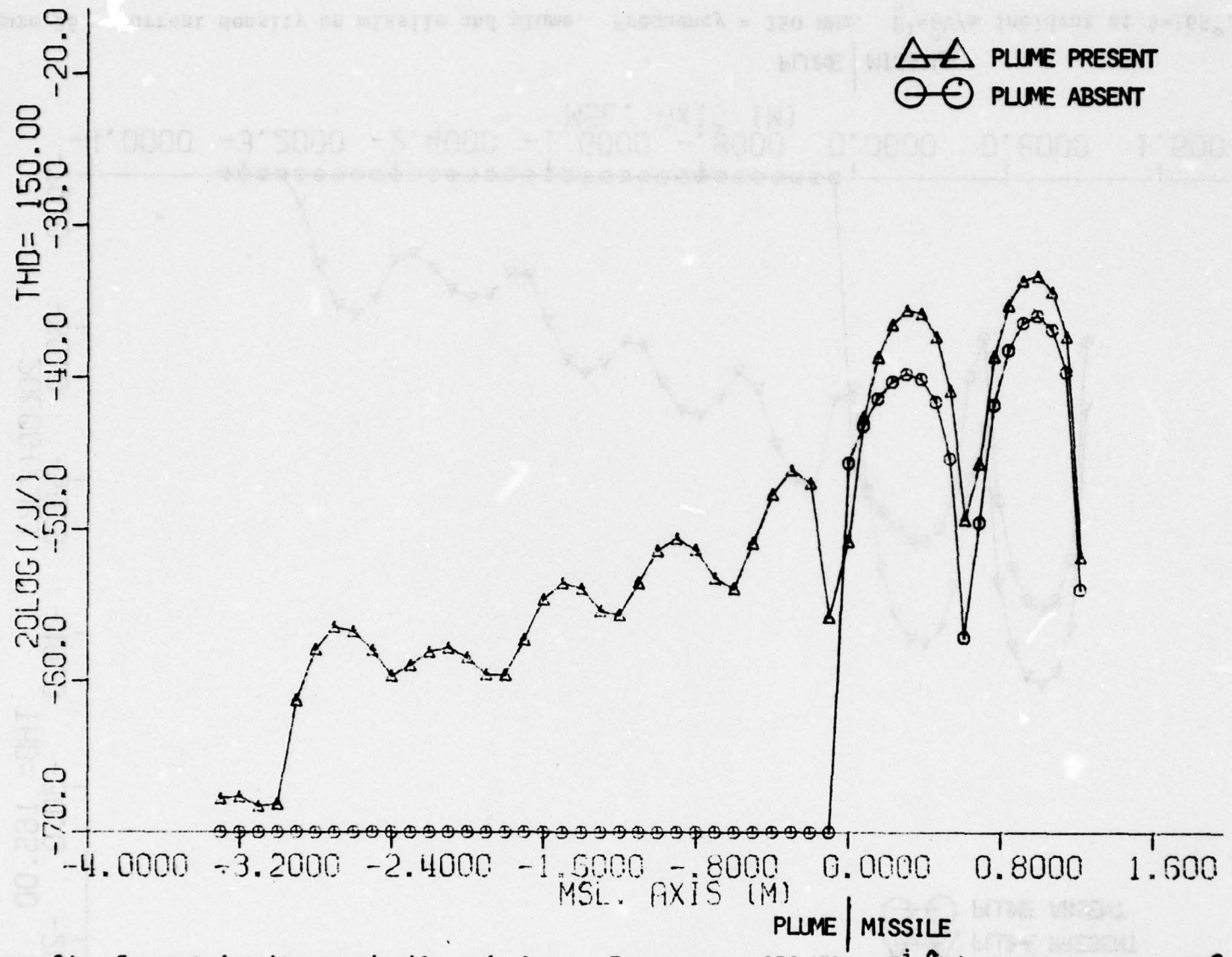

Figure 24. Current density on missile and plume. Frequency = 250 MHz. $\underset{\sim}{E}^{i}=\hat{\theta}$V/m incident at $\theta=150°$.

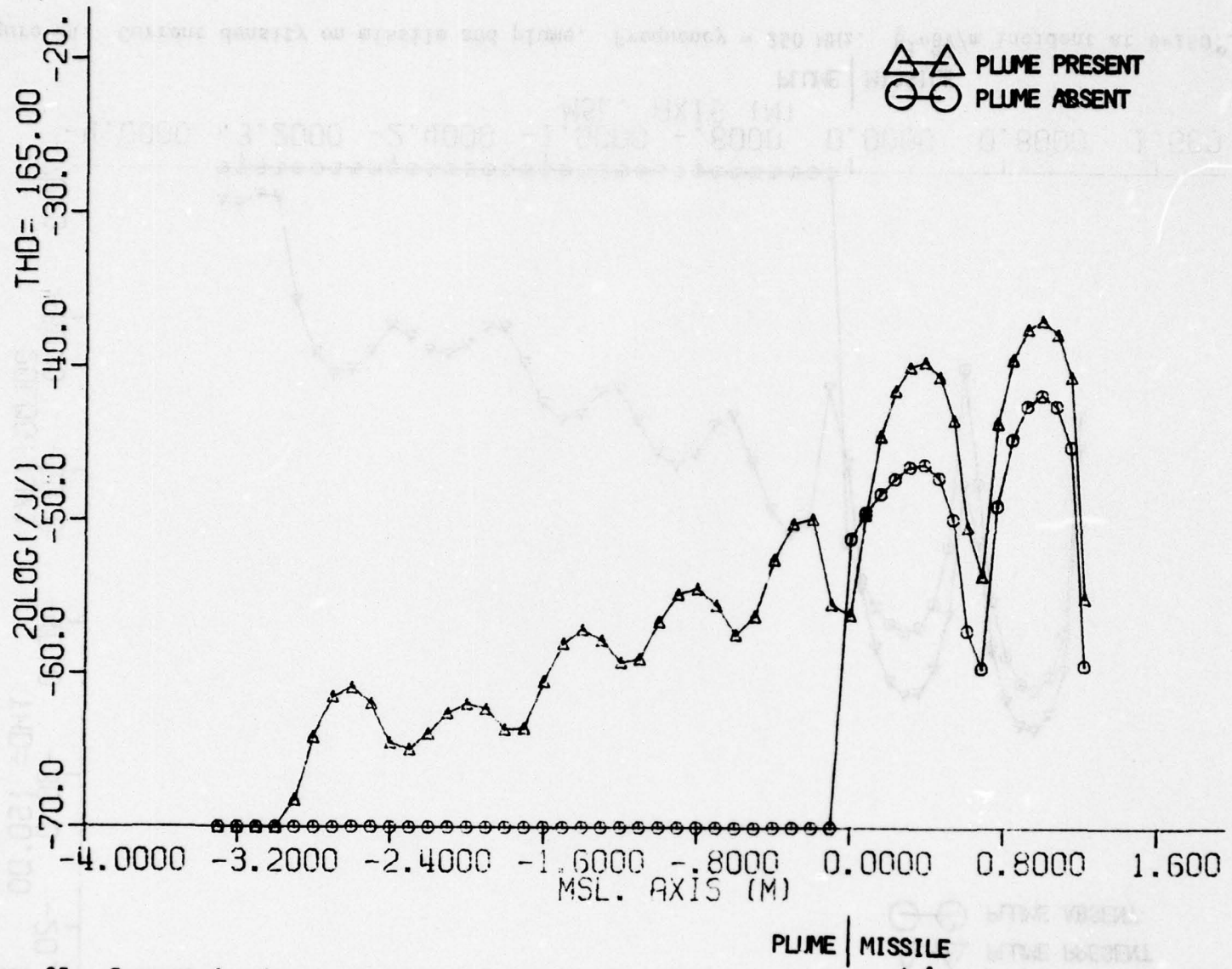

Figure 25. Current density on missile and plume. Frequency = 250 MHz. $\underset{\sim}{E}^{i}=\hat{\theta}$V/m incident at $\theta=165°$.

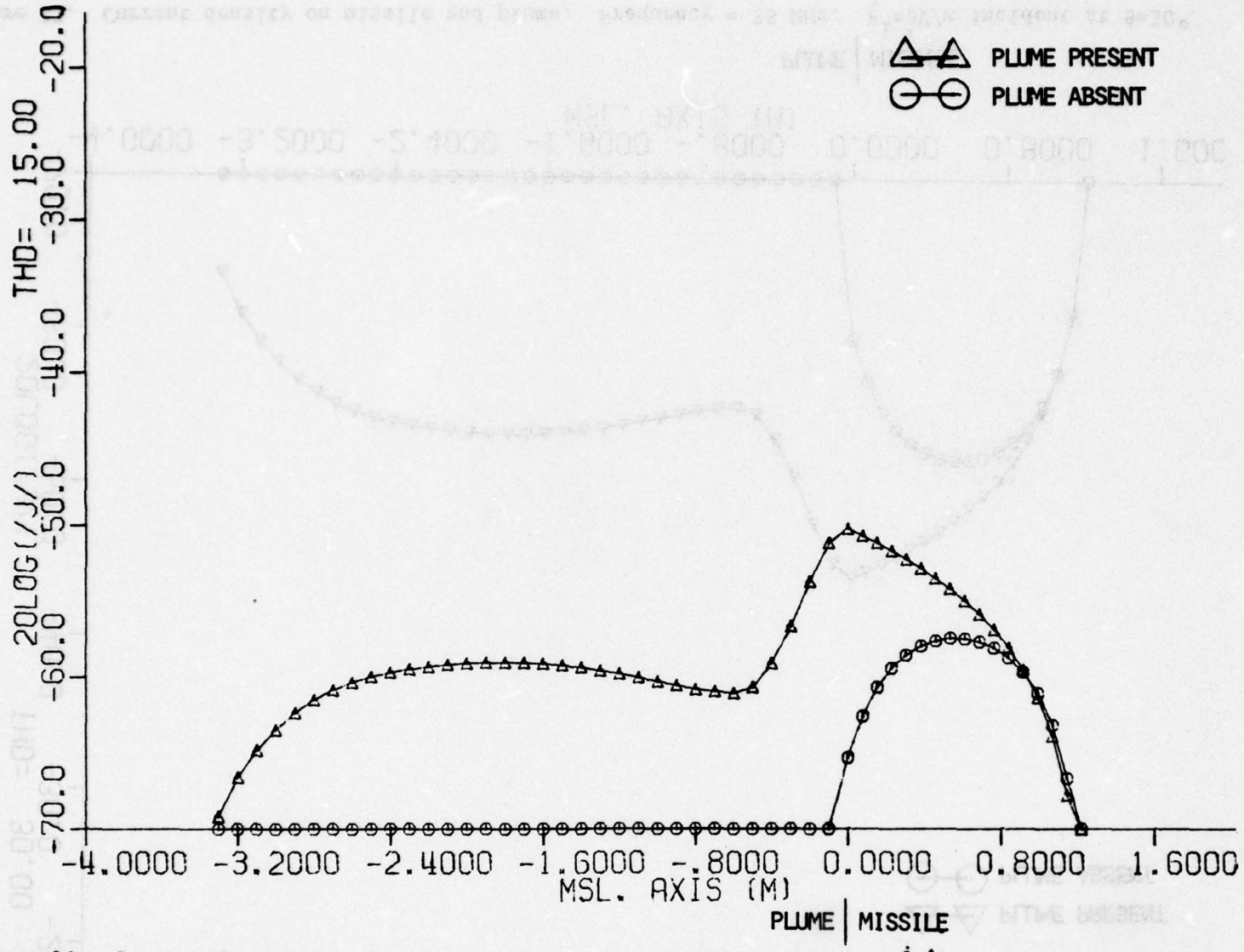

Figure 26. Current density on missile and plume. Frequency = 25 MHz. $\underset{\sim}{E}^{i}=\hat{\theta}$V/m incident at $\theta=15^{\circ}$.

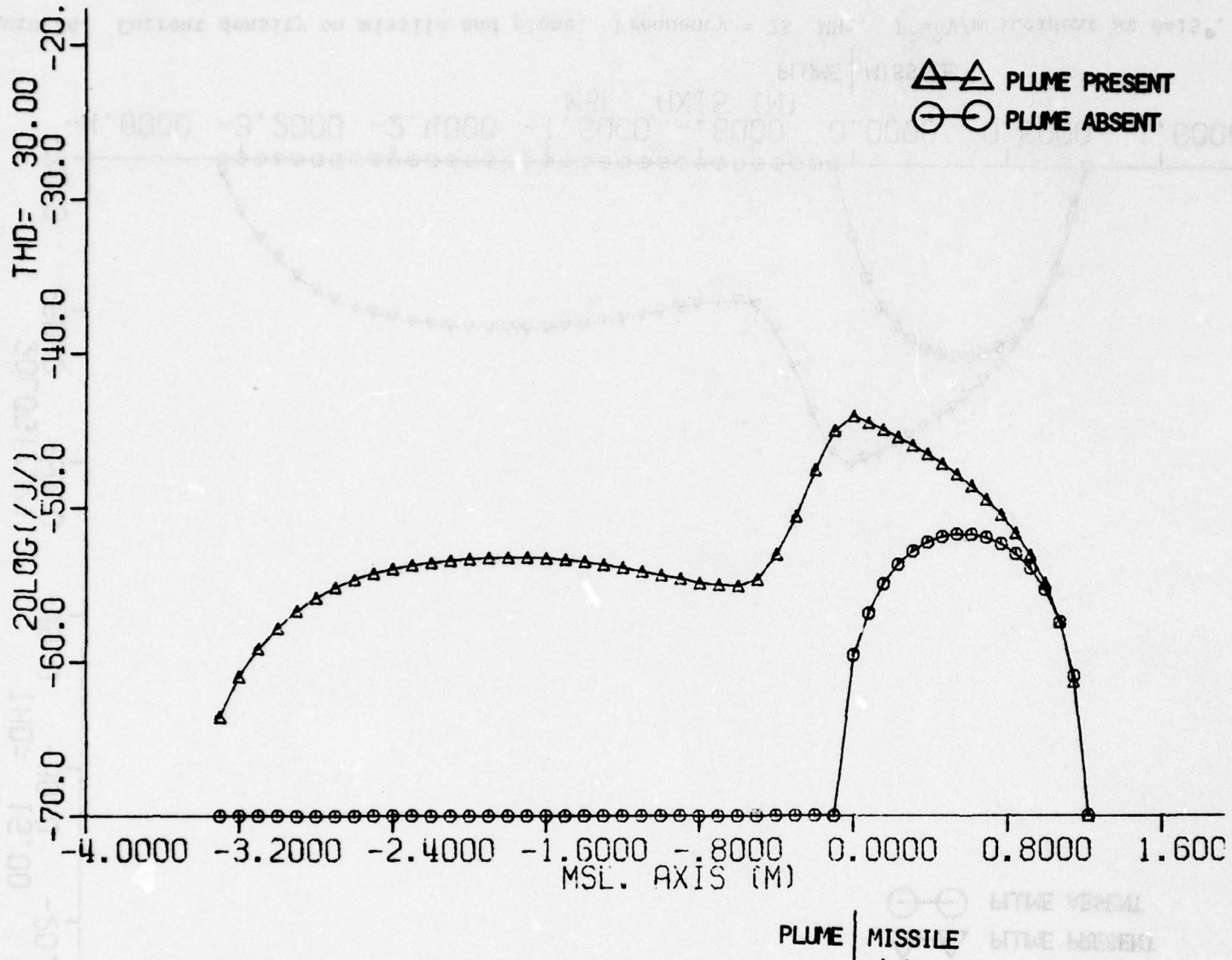

Figure 27. Current density on missile and plume. Frequency = 25 MHz. $\tilde{E}^{i}=\hat{\theta}$V/m incident at $\theta=30°$.

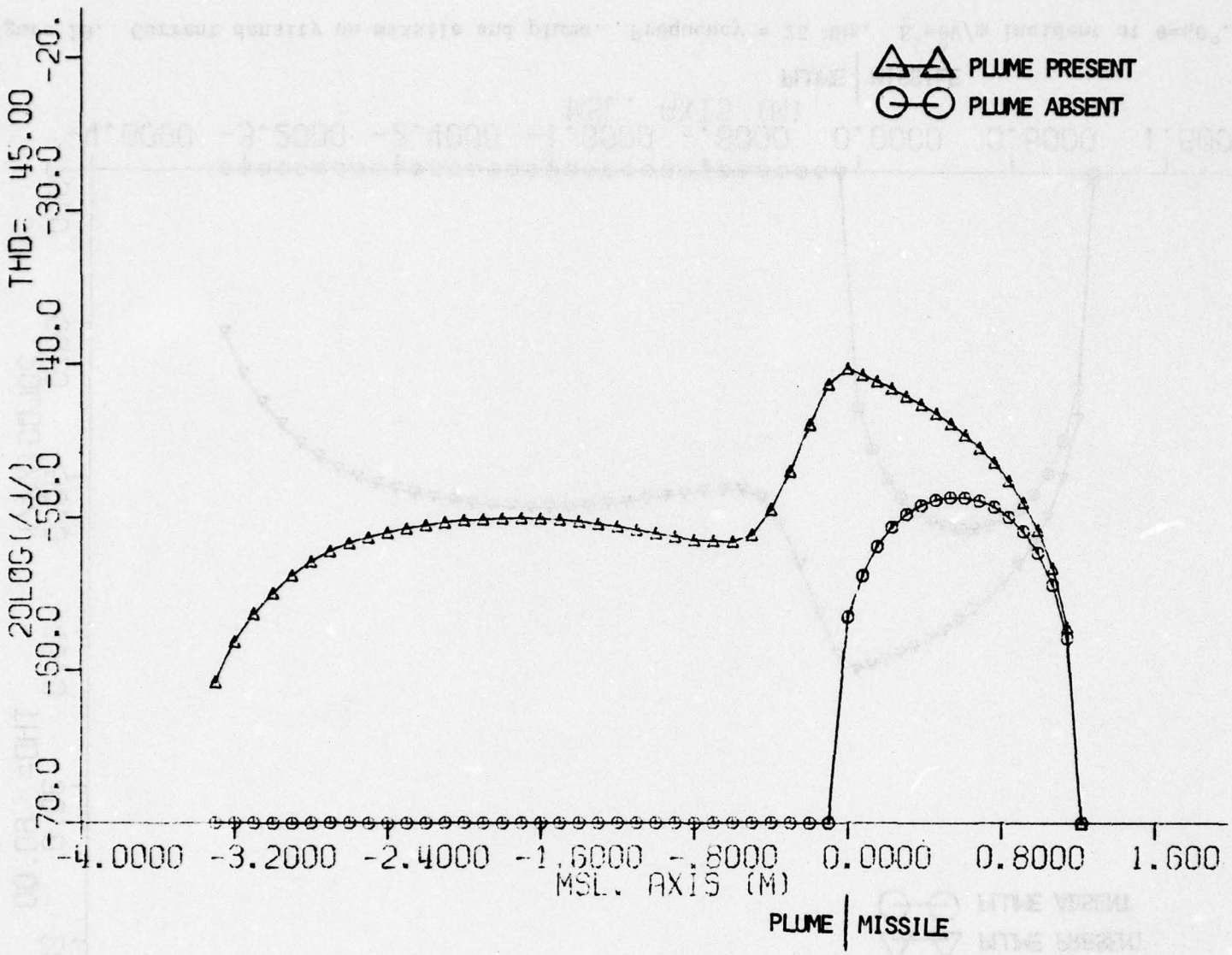

Figure 28. Current density on missile and plume. Frequency = 25 MHz. $\underset{\sim}{E}^{i}=\hat{\theta}$V/m incident at $\theta=45°$.

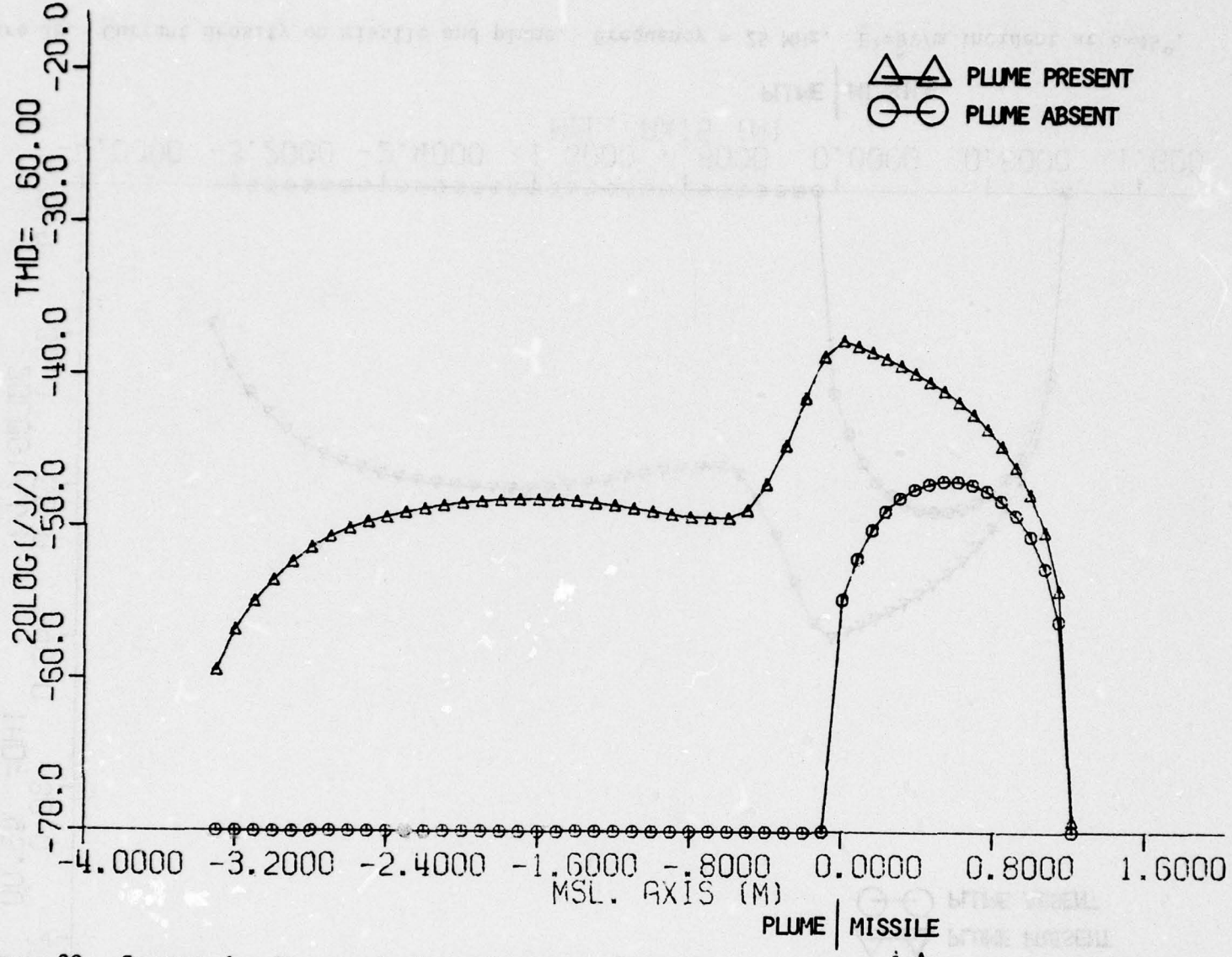

Figure 29. Current density on missile and plume. Frequency = 25 MHz. $\tilde{E}^i = \hat{\theta}$V/m incident at θ=60°.

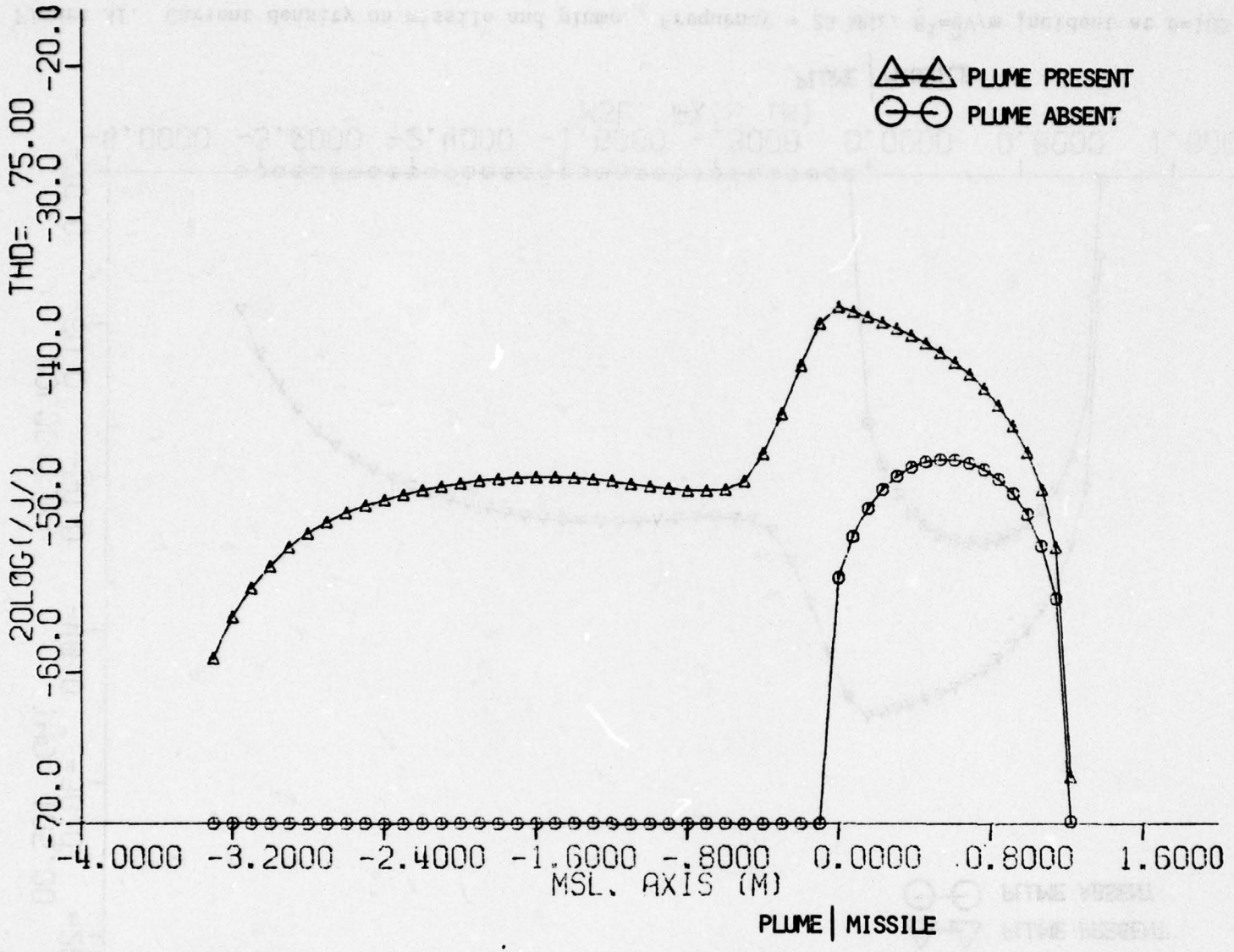

Figure 30. Current density on missile and plume. Frequency = 25 MHz. $\underset{\sim}{E}^i = \hat{\theta}$V/m incident at $\theta=75°$.

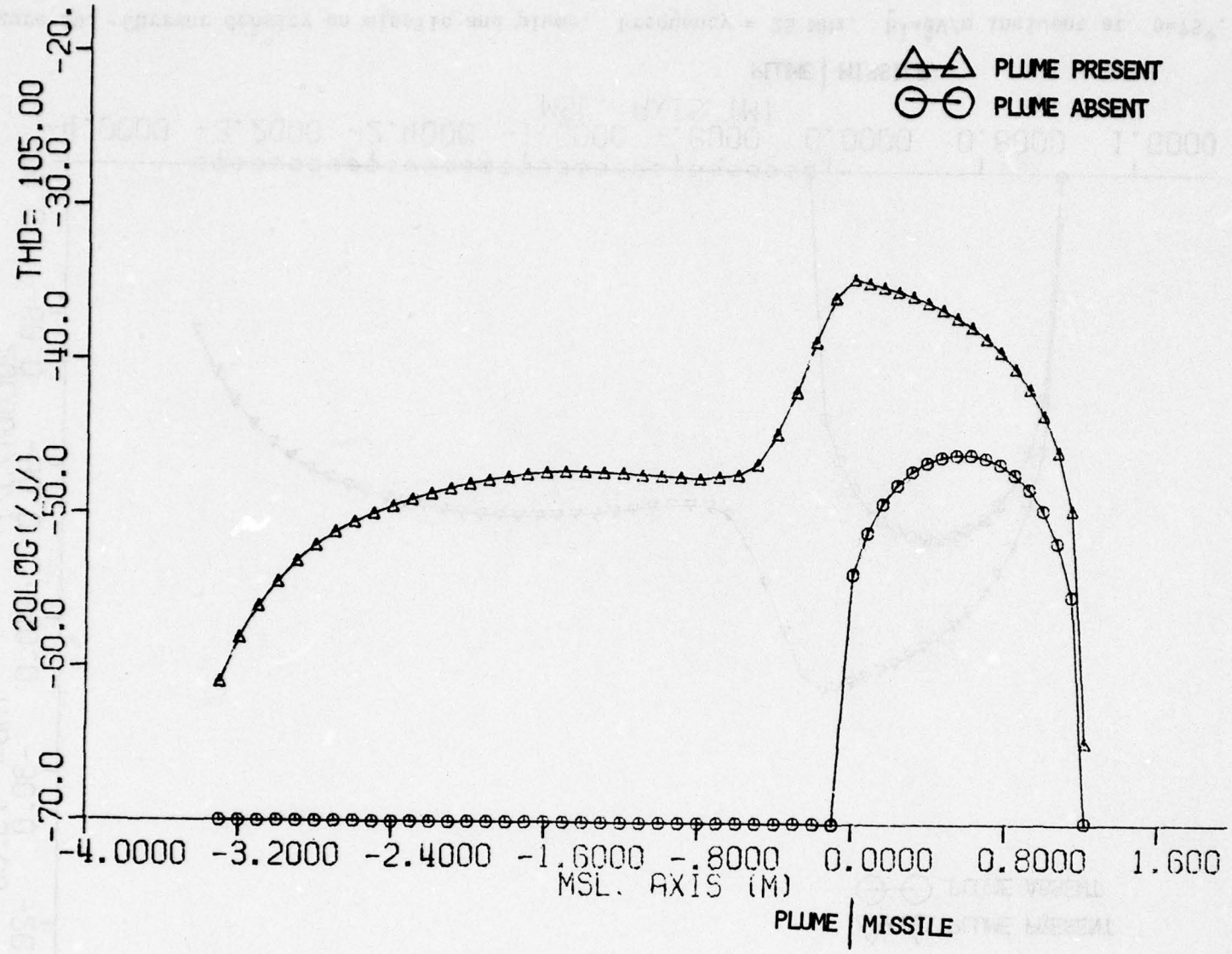

Figure 31. Current density on missile and plume. Frequency = 25 MHz. $\underset{\sim}{E}^i=\hat{\theta}$V/m incident at $\theta=105°$.

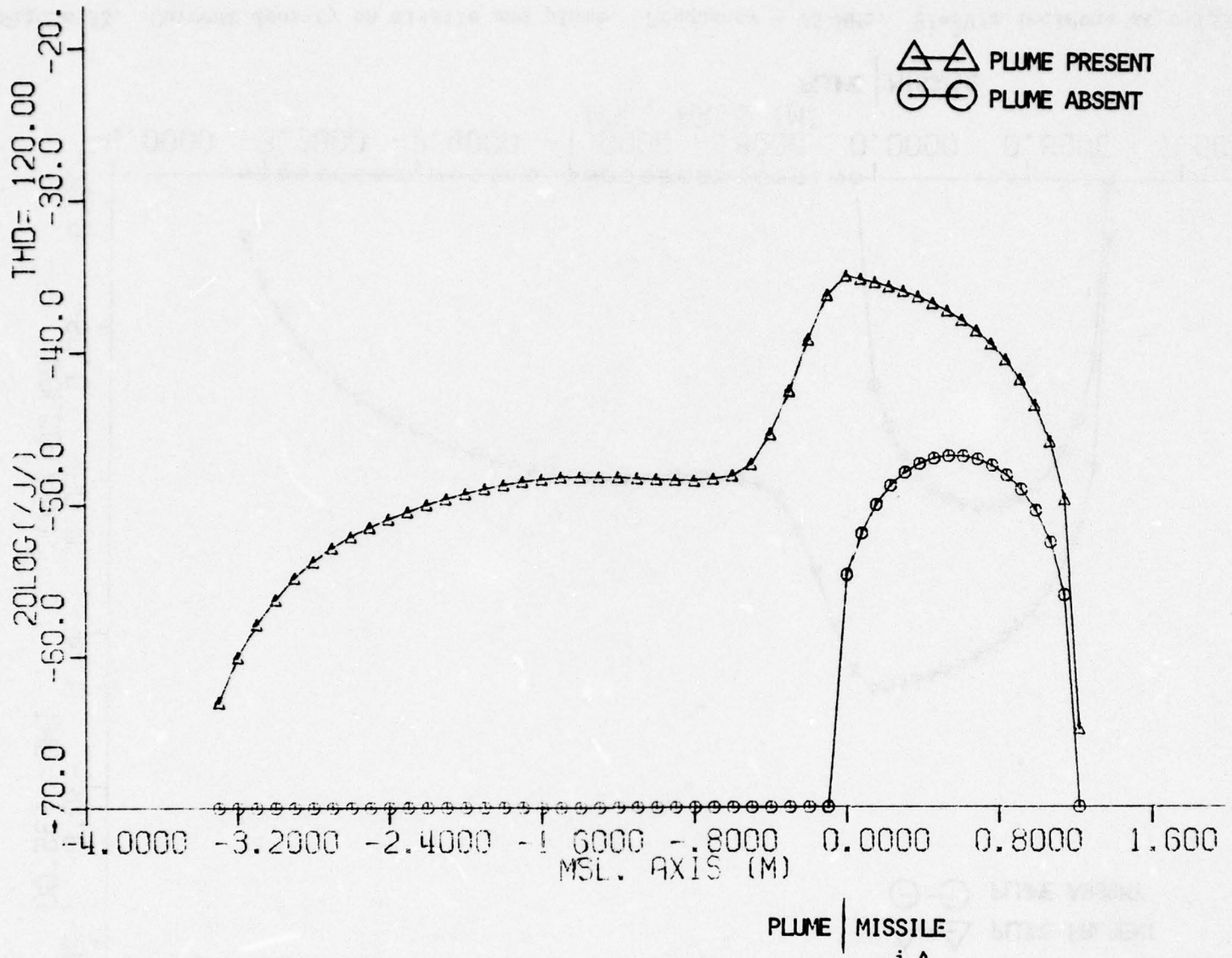

Figure 32. Current density on missile and plume. Frequency = 25 MHz. $\tilde{E}^i = \hat{\theta}$V/m incident at $\theta=120°$.

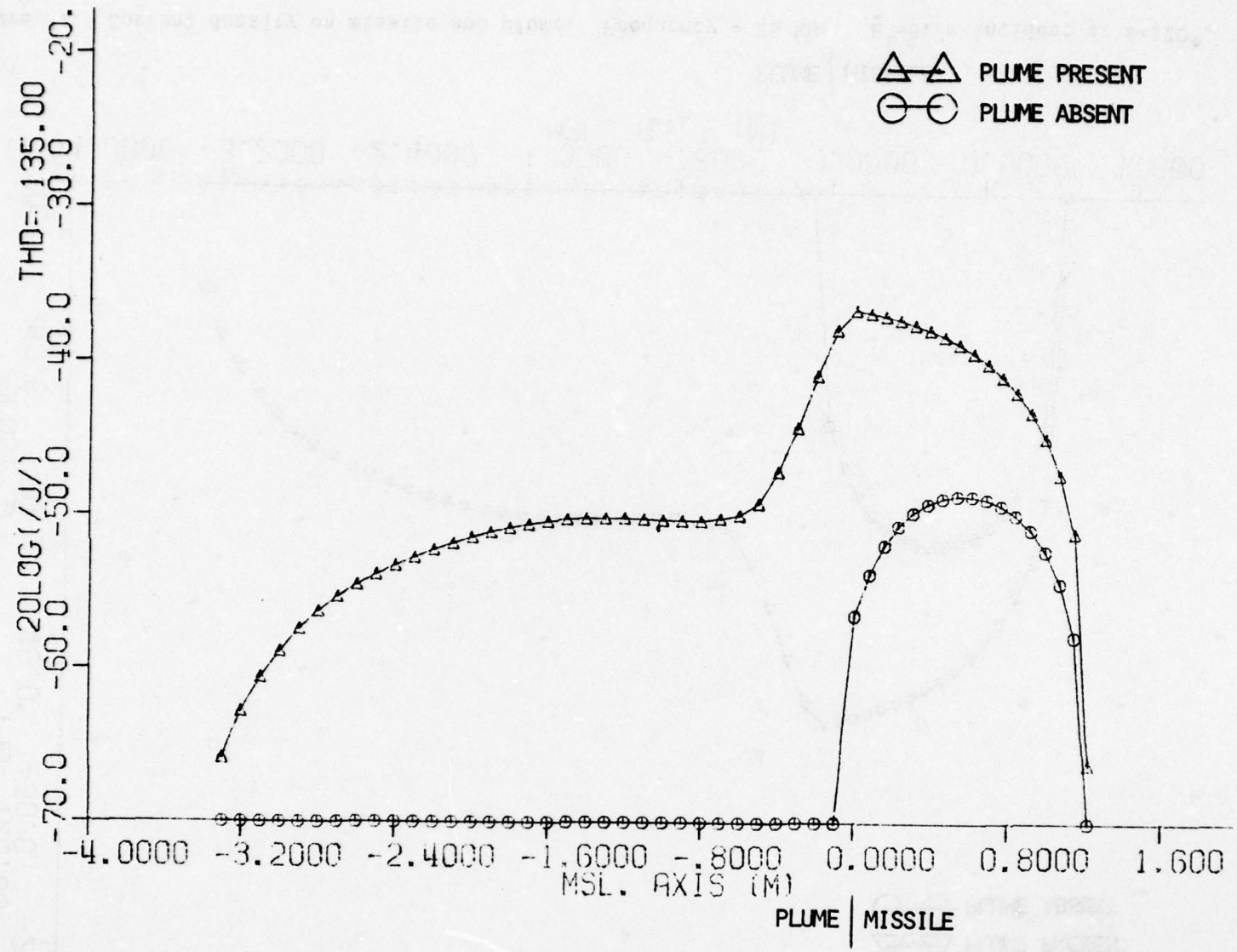

Figure 33. Current density on missile and plume. Frequency = 25 MHz. $\underset{\sim}{E}^i = \hat{\theta}$V/m incident at θ=135°.

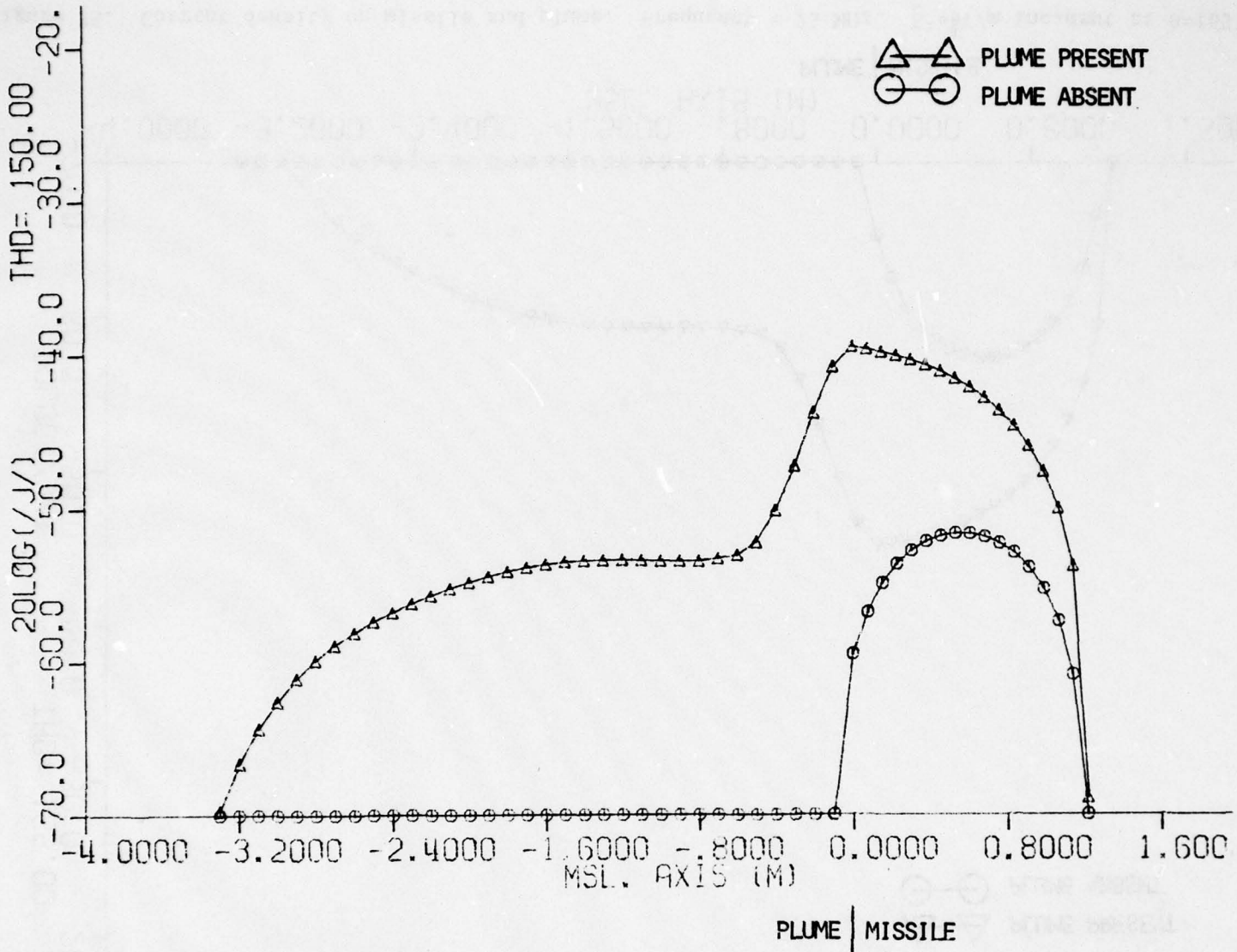

Figure 34. Current density on missile and plume. Frequency = 25 MHz. $\tilde{E}^i = \hat{\theta}$V/m incident at θ=150°.

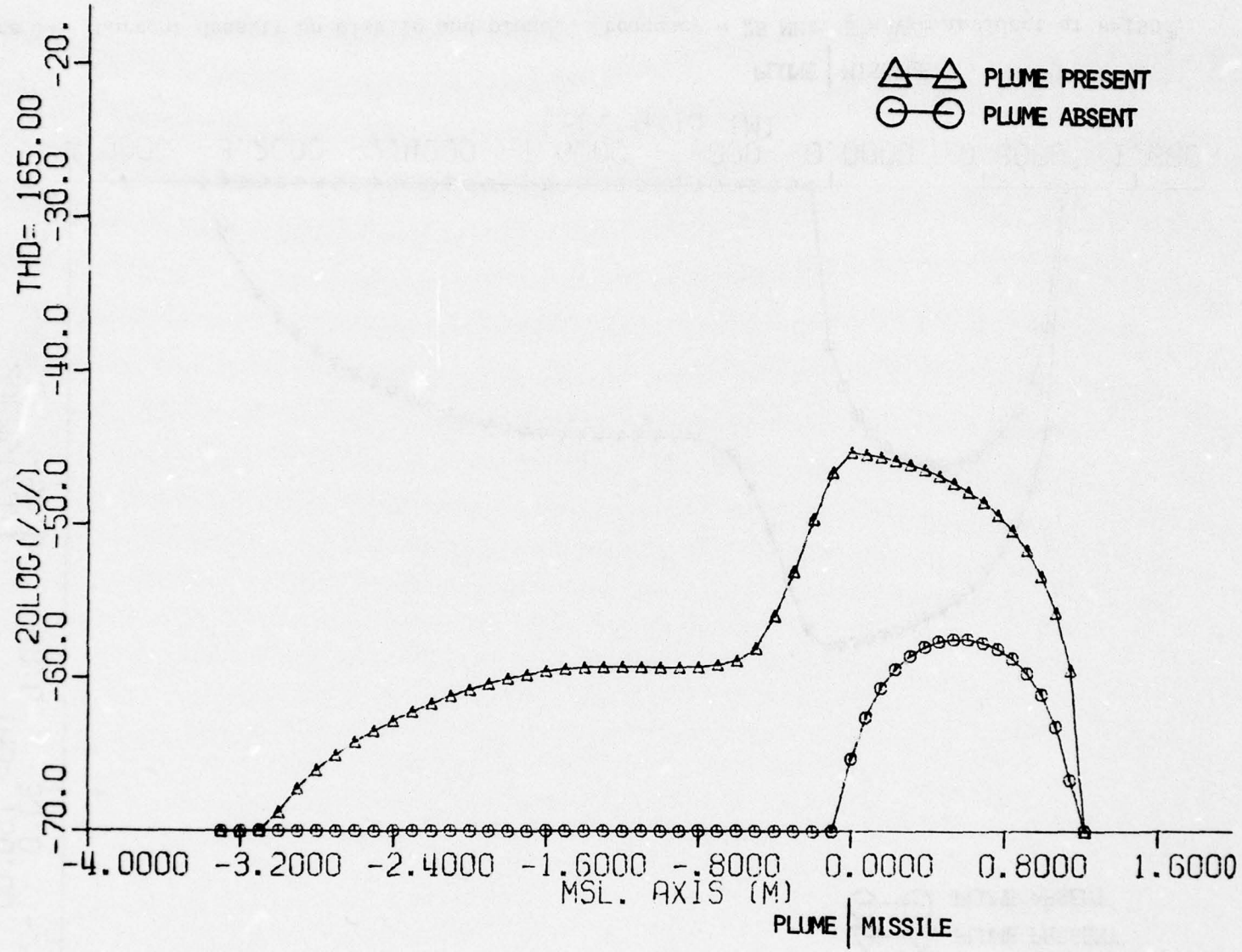

Figure 35. Current density on missile and plume. Frequency = 25 MHz. $\underset{\sim}{E}^i = \hat{\theta}$V/m incident at $\theta=165^\circ$.

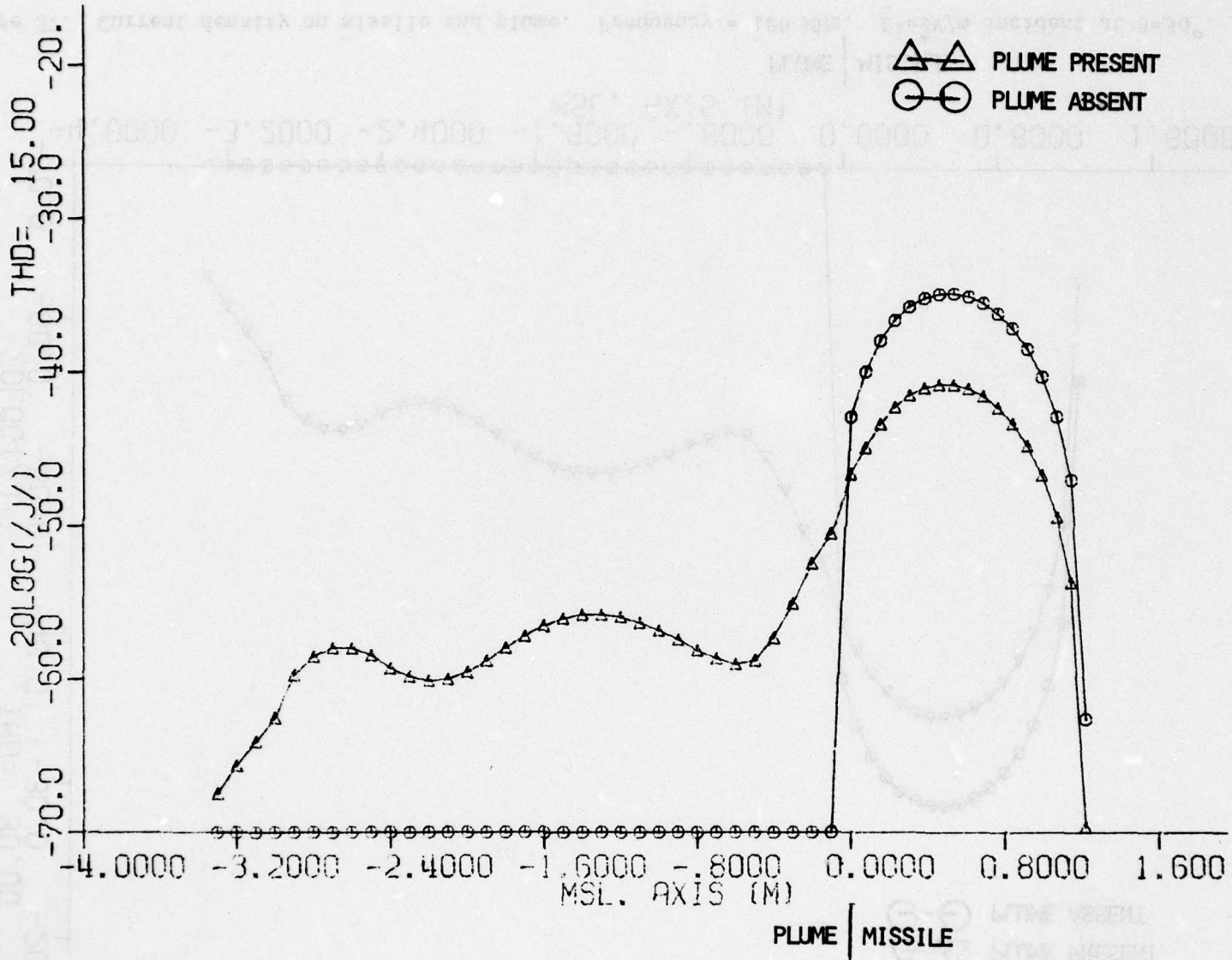

Figure 36. Current density on missile and plume. Frequency = 100 MHz. $\underset{\sim}{E}^{i}=\hat{\theta}$V/m incident at $\theta=15^{o}$.

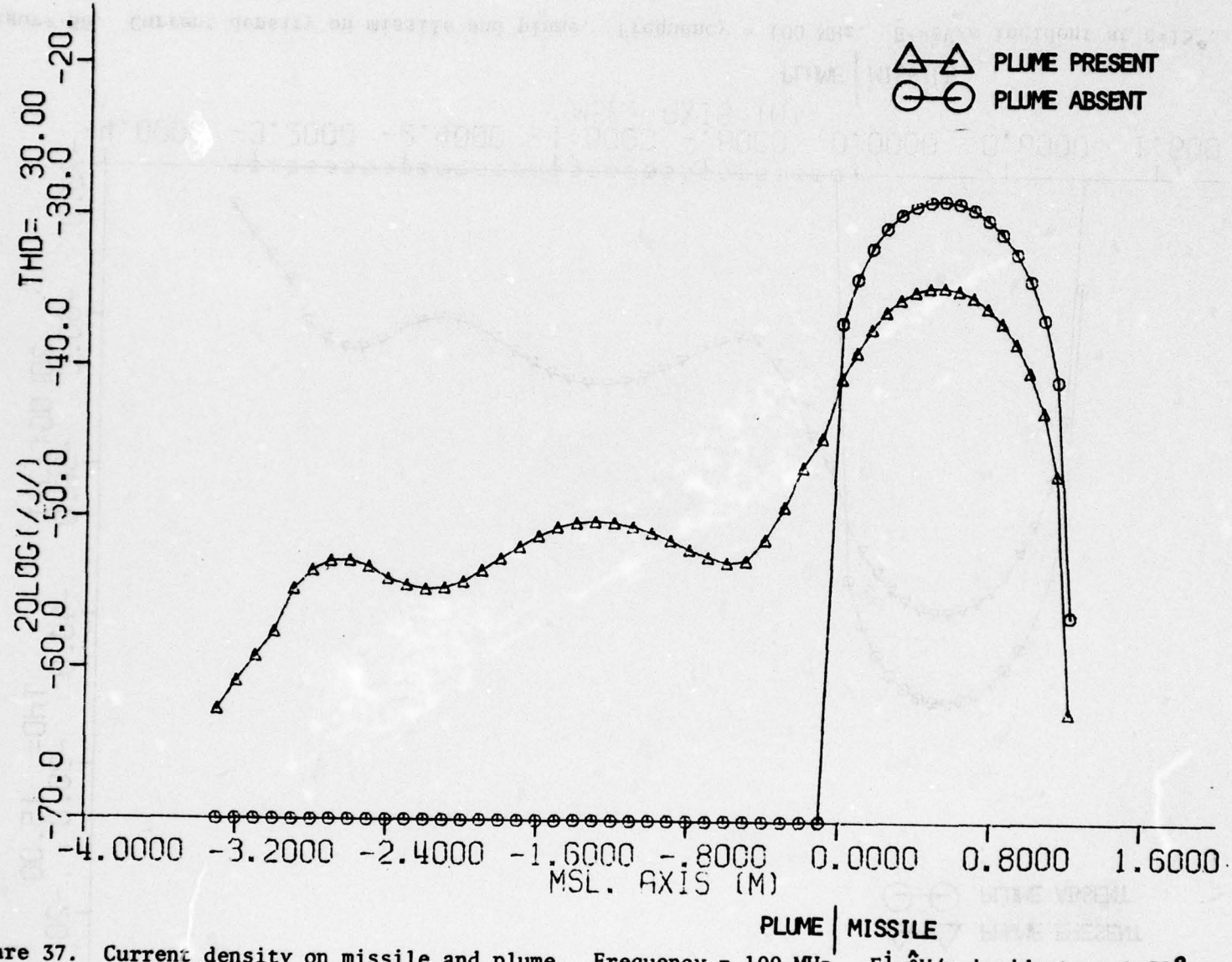

Figure 37. Current density on missile and plume. Frequency = 100 MHz. $\underset{\sim}{E}^i = \hat{\theta}$V/m incident at $\theta=30°$.

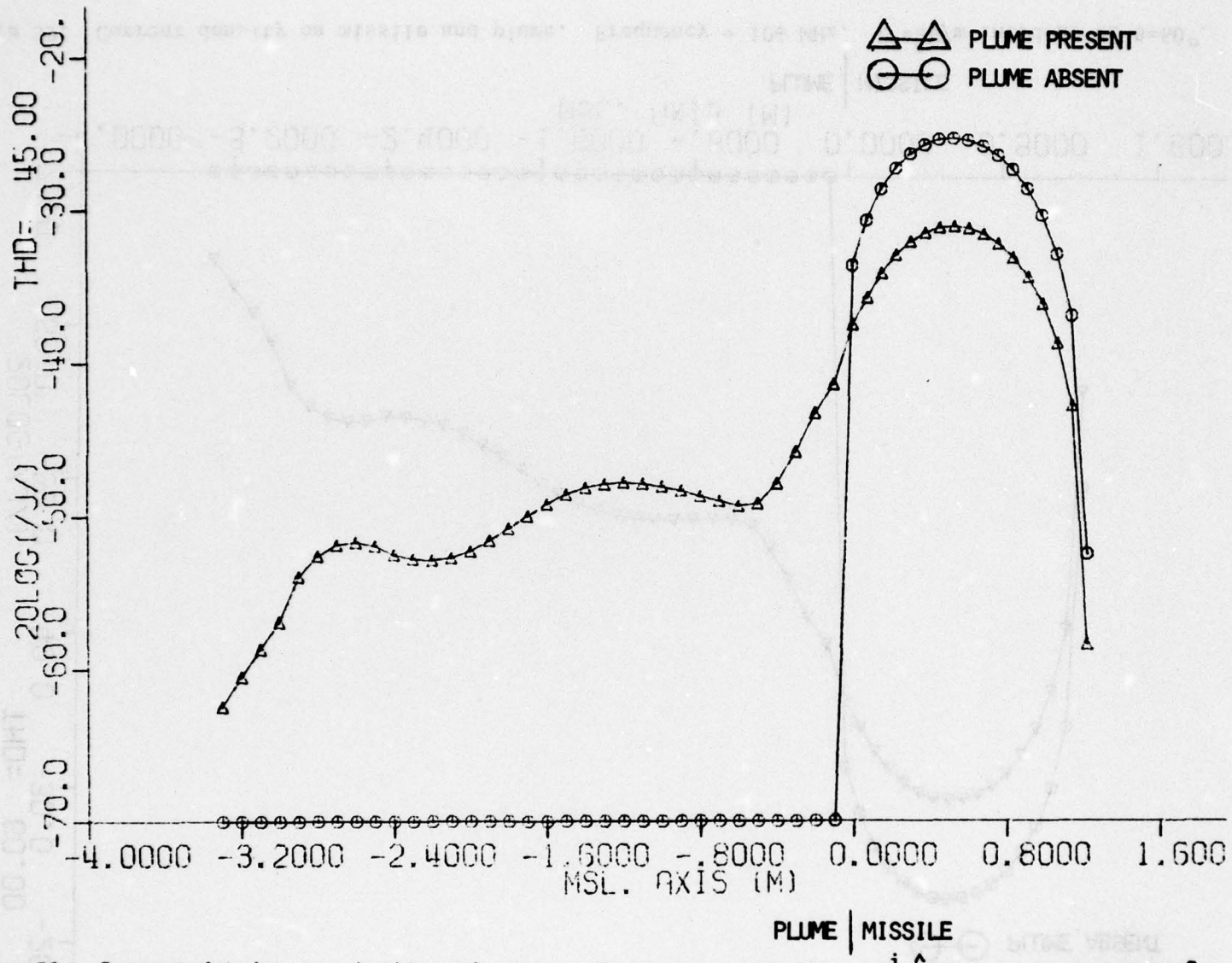

Figure 38. Current density on missile and plume. Frequency = 100 MHz. $\underset{\sim}{E}^{i}=\hat{\theta}$V/m incident at $\theta=45°$.

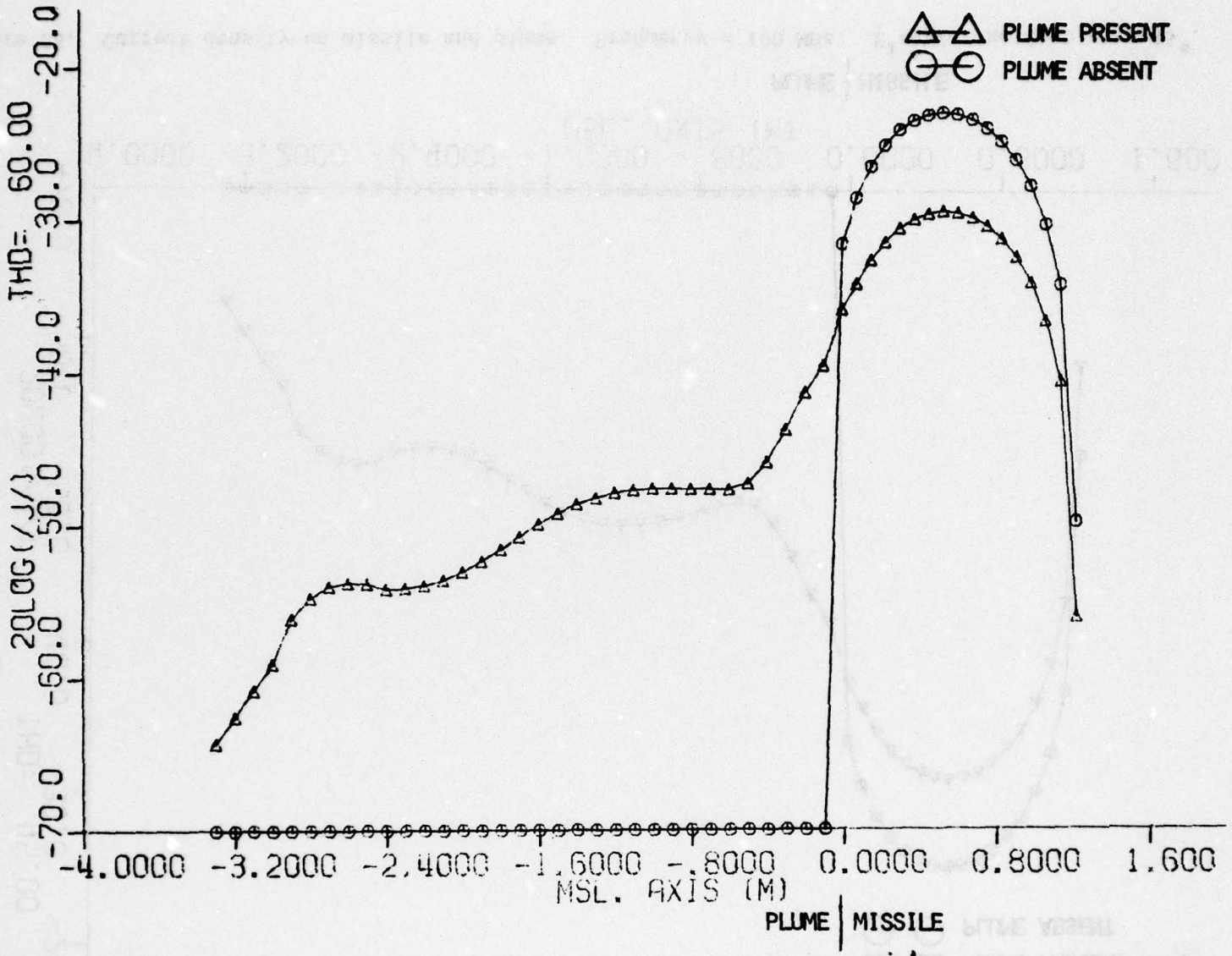

Figure 39. Current density on missile and plume. Frequency = 100 MHz. $\underset{\sim}{E}^{i}=\hat{\theta}$V/m incident at $\theta=60°$.

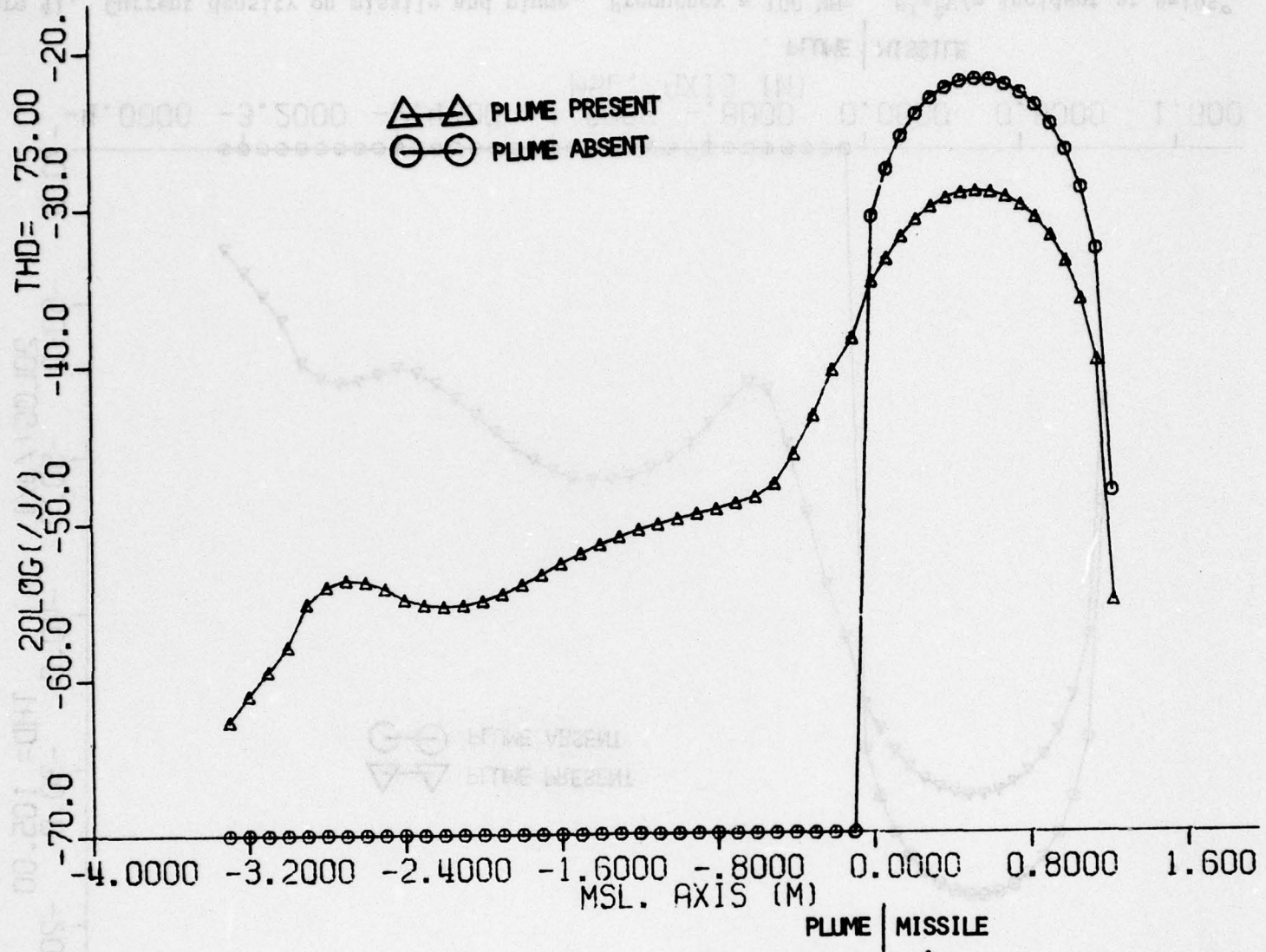

Figure 40. Current density on missile and plume. Frequency = 100 MHz. $\underset{\sim}{E}^{i}=\hat{\theta}$V/m incident at $\theta=75°$.

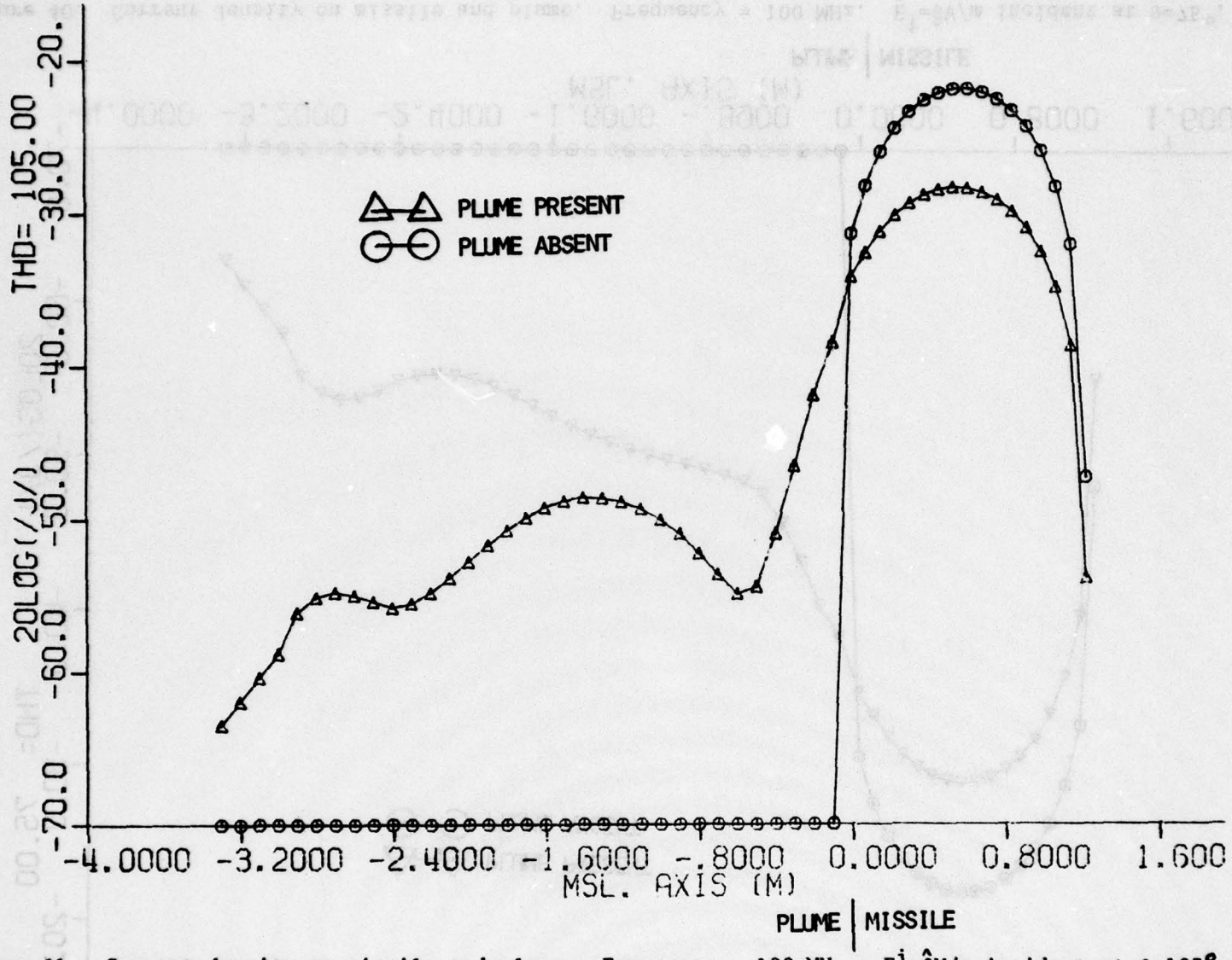

Figure 41. Current density on missile and plume. Frequency = 100 MHz. $\underset{\sim}{E}^{i}=\hat{\theta}$V/m incident at $\theta=105^{\circ}$.

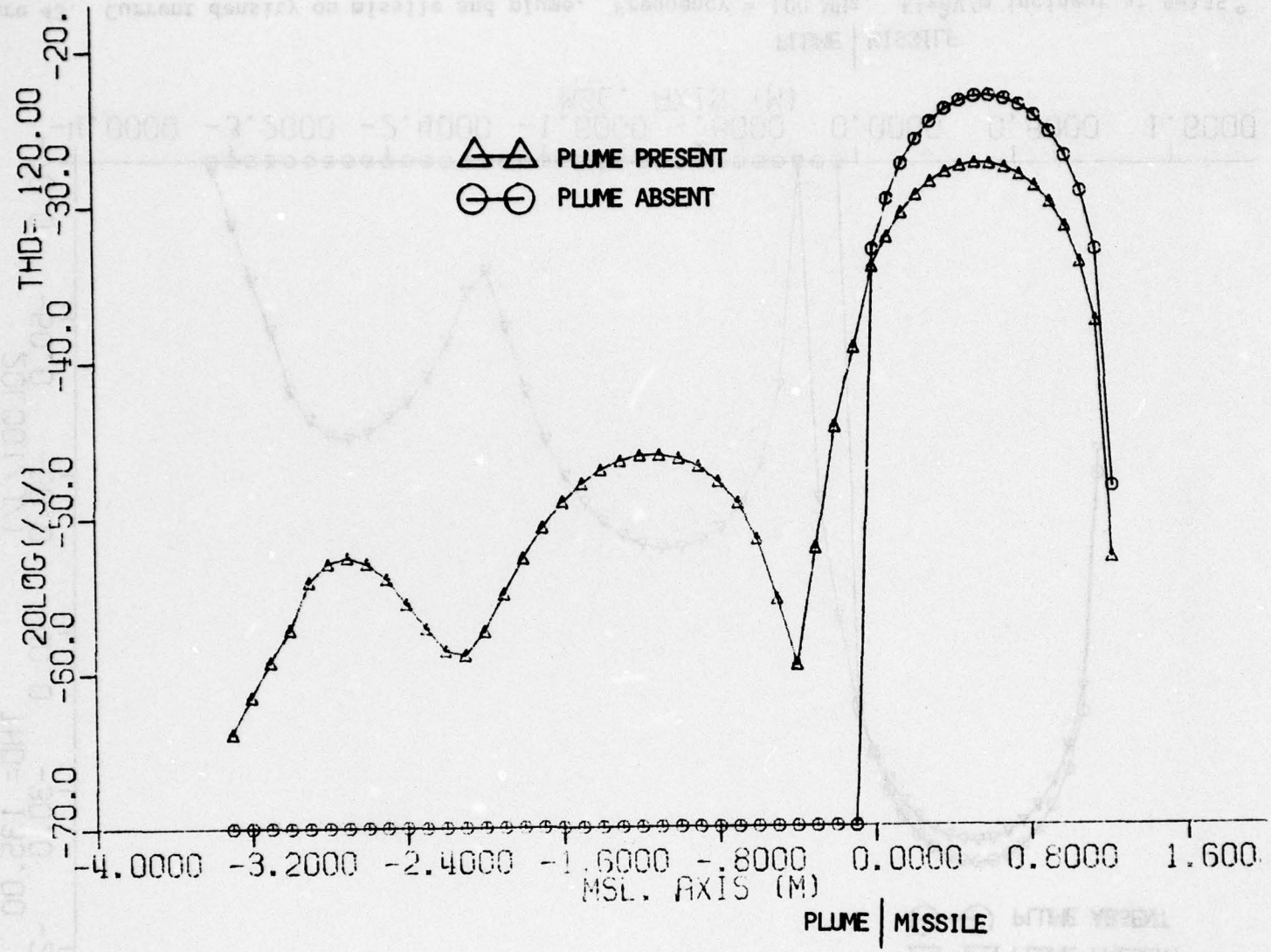

Figure 42. Current density on missile and plume. Frequency = 100 MHz. $\underset{\sim}{E}^i$= 0̈V/m incident at θ=120°

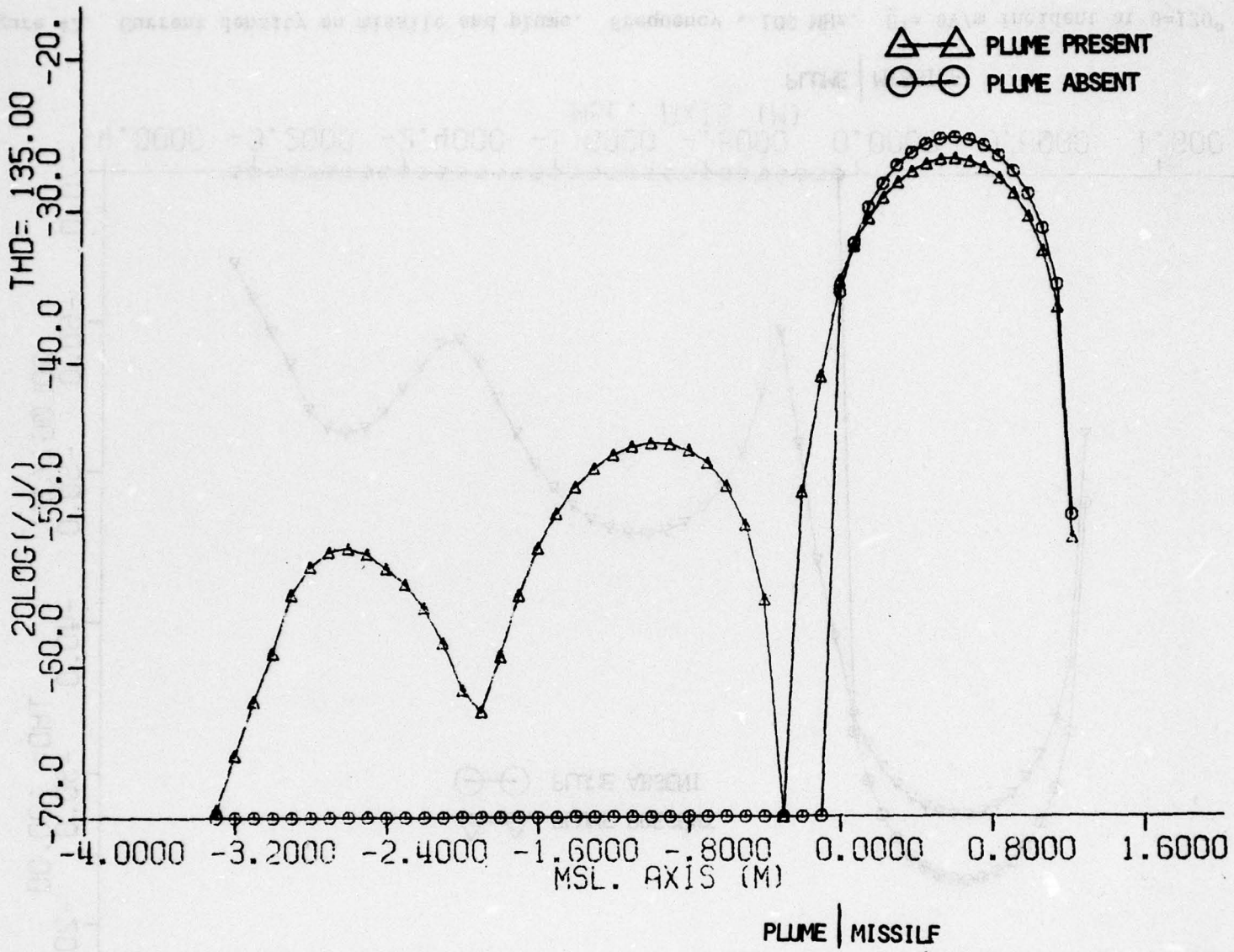

Figure 43. Current density on missile and plume. Frequency = 100 MHz. $\underset{\sim}{E}^i = \hat{\theta}$V/m incident at $\theta = 135°$.

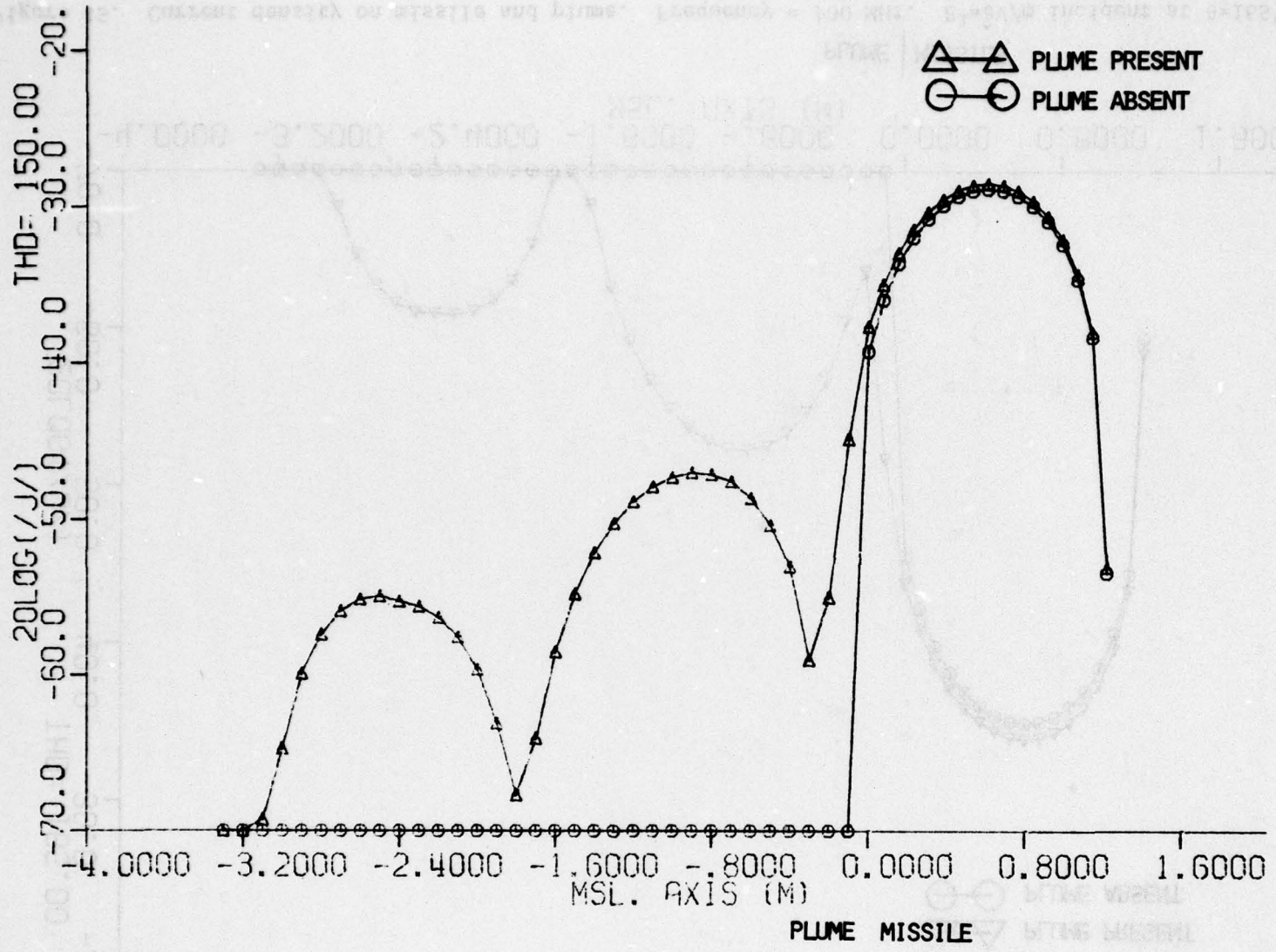

Figure 44. Current density on missile and plume. Frequency = 100 MHz. $\underset{\sim}{E}^{i}=\hat{\theta}$V/m incident at $\theta=150^{\circ}$.

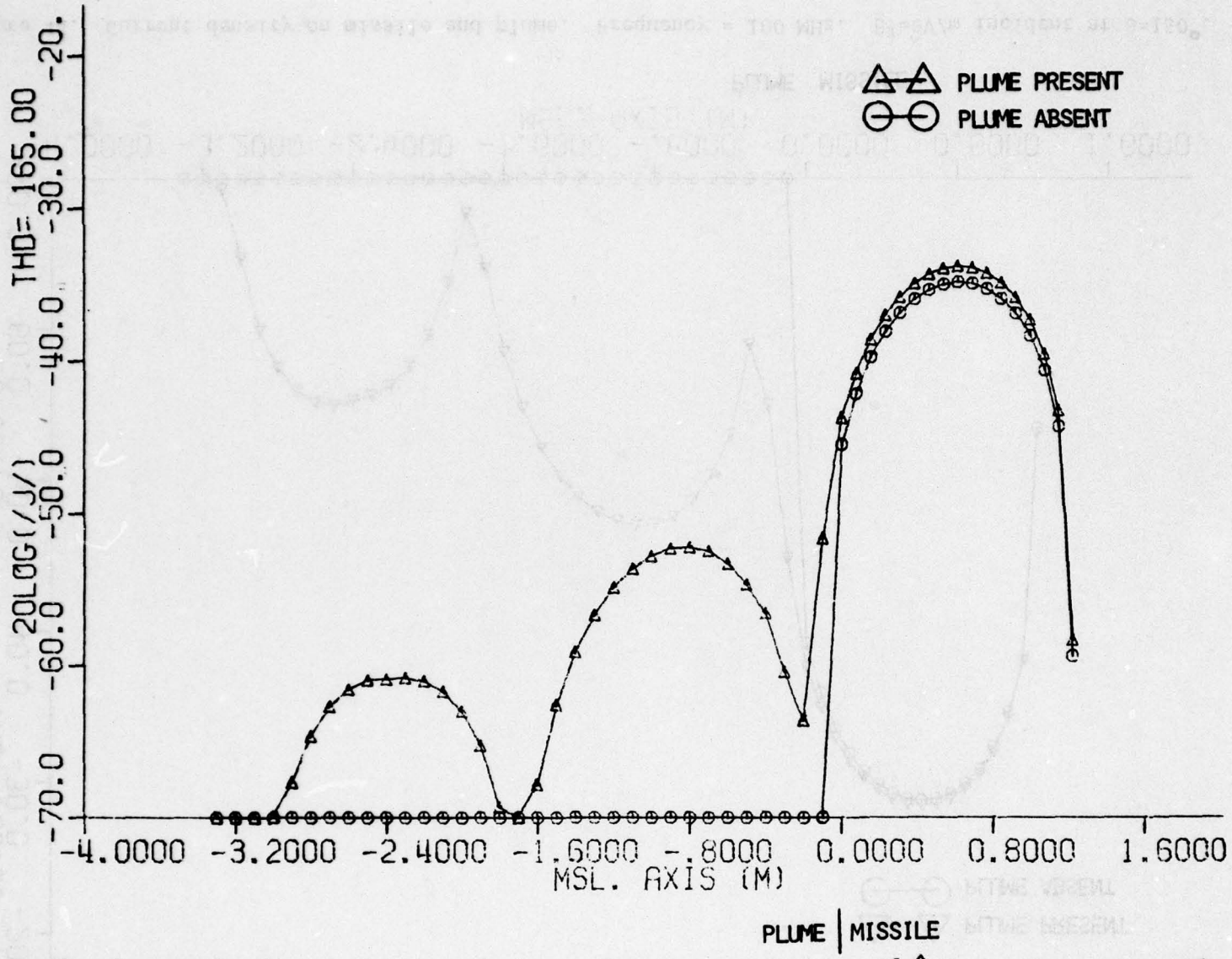

Figure 45. Current density on missile and plume. Frequency = 100 MHz. $\underset{\sim}{E}^{i}=\hat{\theta}$V/m incident at $\theta=165^{\circ}$.

small for θ between near broadside and near nose-end incidence ($15° \leq \theta \leq 75°$). The plume effect is significant for values of θ between near broadside and near tail-end incidence ($105° \leq \theta \leq 165°$) except in the vicinity of θ=135°. The peak effect occurs at θ=165° (Figure 25) where the plume <u>increases</u> $|J_{sc}|$ by ~6.5 dB at some points along the missile surface.

The plume effect at the low-frequency end (f=25 MHz, $L \approx 0.1\lambda$) is again greater for $105° \leq \theta \leq 165°$ than for $15° \leq \theta \leq 75°$. This is apparent in Figures 26-35. For all θ the plume effect is to greatly increase the missile current near the tail. At the location of peak current on the plume-absent missile a maximum current increase of about 10 dB is introduced by plume presence. This occurs at θ=165° (Figure 35).

In contrast with the above, at resonance (f=100 MHz, $L \approx 0.4\lambda$) the plume effect is greatest for incidence angles between broadside and near nose-end ($15° \leq \theta \leq 90°$). Also, plume presence now reduces the current at all points on the missile surface except very near the tail. The peak reduction is ~7 dB which occurs near θ=90°.

5. Conclusions

The effects of a resistive exhaust plume on the scattering currents induced on a thin missile have been discussed. This work supplements concurrent work recently reported in [8] which relied on the thin-wire approximation for modeling both missile and plume. The model used here was derived from body-of-revolution theory [1,2] and the impedance-sheet concept [3]. These theories enabled, in particular, the significant width of the plume, about eight times the missile diameter, to be accounted for with a

correspondingly wide model. Both efforts show reasonable agreement in predicting missile current distributions and levels for low, resonance and above-resonance frequencies at broadside incidence excitation. One significant difference for broadside excitation is that the model used here predicts ~3 dB greater plume effect at the location on the missile body of peak current at resonance. The plume effect here is a reduction in missile current by ~7 dB.

Plume effects on cavity fields within the missile can be assessed directly from the data presented. This is especially true if the apertures through which energy is coupled are small. In this case the internal fields are proportional to the missile currents (magnetic dipole coupling) and current slopes (electric dipole coupling) in the vicinity of the apertures after shorting [7].

Other significant aspects of the plume effects as predicted by this work are summarized below.

1. Resonance - This is the only frequency region where a significant reduction in missile current is experienced.
2. Low frequency - For a 0.1λ long missile the surface current is greatly increased especially near the tail (thruster). The largest plume effect (even excluding the tail region) occurs at this frequency and for near tail-end incidence. The increase in current is then ~10 dB at the location of peak plume-absent current. However, at locations other than the tail the absolute peak current levels with or without the plume are significantly below those of the

resonance case. Hence, excluding pertinent apertures near the tail, cavity fields at low frequencies will generally be less than at external resonance frequencies.

3. Above resonance - For a wavelength long missile under broadside excitation the missile current peaks are shifted slightly. However, for near tail-end incidence the currents are increased by ~6.5 dB at some points along the missile surface. Also one notes that the shifting, even slightly, of severe current slopes could result in large cavity field variations.

REFERENCES

[1]. R.F. Harrington and J.R. Mautz, "Radiation and Scattering from Bodies of Revolution," Final Report, prepared for Air Force Cambridge Research Laboratories, Bedford, Mass., under Contract No. F19628-67-C-0233, July 1969.

[2]. J.R. Mautz and R.F. Harrington, "Generalized Network Parameters for Bodies of Revolution," Scientific Report No. 1, Contract No. F19628-67-C-0233, Air Force Cambridge Research Laboratories, Bedford, Mass., with Syracuse University, Syracuse, N.Y., May 1968. Or see instead: J.R. Mautz and R.F. Harrington, "Radiation and Scattering from Bodies of Revolution," Applied Scientific Research, Vol. 20, 1969.

[3]. R.F. Harrington and J.R. Mautz, "An Impedance Sheet Approximation for Thin Dielectric Shells", IEEE Transactions on Antennas and Propagation, vol. AP-23, pp. 531-534, July 1975.

[4]. T.K. Wu, "Electromagnetic Scattering from Arbitrarily-Shaped Lossy Dielectric Bodies," PhD dissertation, Univ. of Miss., May 1976.

[5]. R.F. Harrington, Field Computation by Moment Methods, The Macmillan Co., New York, 1968.

[6]. J.D. Nordgard and G.S. Smith, "A Plasma Model of Missile Exhaust Plumes. (Axial and Radial Conductivity Distributions for the Redeye Missile)". TR-77-144, Rome Air Development Center, Griffiss Air Force Base, New York, April 1977, AD# A040057.

[7]. H.K. Schuman, "Circumferential Distribution of Scattering Current and Small Hole Coupling for Thin Finite Cylinders," Rome Air Development Center, Griffiss AFB, technical report under Contract F30602-75-C-0121 of the RADC Post-Doctoral Program with Syracuse University, circa Dec. 1977, RADC-TR-77-412.

[8]. G.S. Smith, J.D. Nordgard, and J. Edwards, "Alteration of the Surface Current on a Missile by the Presence of an Exhaust Plume," IEEE Transactions on Electromagnetic Compatibility, vol. EMC-19, pp. 19-30, Nov. 1977.

MISSION
of
Rome Air Development Center

RADC plans and conducts research, exploratory and advanced development programs in command, control, and communications (C^3) activities, and in the C^3 areas of information sciences and intelligence. The principal technical mission areas are communications, electromagnetic guidance and control, surveillance of ground and aerospace objects, intelligence data collection and handling, information system technology, ionospheric propagation, solid state sciences, microwave physics and electronic reliability, maintainability and compatibility.